

1 **Neurodegeneration and neuroinflammation are linked, but independent of  $\alpha$ -synuclein**  
2 **inclusions, in a seeding/spreading mouse model of Parkinson's disease**

3

4 Pierre Garcia\*<sup>1,2</sup>, Wiebke Jürgens-Wemheuer\*<sup>1,7</sup>, Oihane Uriarte\*<sup>1,2</sup>, Kristopher J  
5 Schmit\*<sup>1,2</sup>, Annette Masuch<sup>3</sup>, Simone Brioschi<sup>3</sup>, Andreas Weihofen<sup>4</sup>, Eric Koncina<sup>5</sup>, Djilil  
6 Coowar<sup>1</sup>, Tony Heurtaux<sup>2,5</sup>, Enrico Glaab<sup>1</sup>, Rudi Balling<sup>1</sup>, Carole Sousa<sup>6</sup>, Alessandro  
7 Michelucci<sup>6</sup>, Tony Kaoma<sup>6</sup>, Nathalie Nicot<sup>6</sup>, Tatjana Pfander<sup>7</sup>, Walter Schulz-Schaeffer<sup>7</sup>,  
8 Ahmad Allouche<sup>8</sup>, Nicolas Fischer<sup>8</sup>, Knut Biber<sup>3</sup>, Michel Mittelbronn<sup>1,2,9</sup>, and Manuel  
9 Buttini<sup>1,2</sup>

10 *\*these authors contributed equally to the study*

11 <sup>1</sup> Luxembourg Centre for Systems Biomedicine, University of Luxembourg, L-4362 Esch-sur-Alzette,  
12 Luxembourg; <sup>2</sup> Luxembourg Center of Neuropathology (LCNP), Luxembourg; <sup>3</sup> Department of  
13 Psychiatry, University of Freiburg Medical Center, D-79104 Freiburg, Germany; <sup>4</sup> Biogen ,  
14 Cambridge, MA 02142, USA; <sup>5</sup> Department of Life Science and Medicine, University of  
15 Luxembourg, L-4362 Esch-sur-Alzette, Luxembourg; <sup>6</sup> Luxembourg Institute of Health, L-1445  
16 Strassen, Luxembourg; <sup>7</sup> Institute of Neuropathology, Saarland University Clinic (UKS), D-66421  
17 Homburg, Germany; <sup>8</sup> SynAging SAS, 54500 Vandœuvre-lès-Nancy, France; <sup>9</sup> National Center of  
18 Pathology (NCP), Laboratoire National de Santé (LNS), L-3555 Dudelange, Luxembourg.

19 *Current addresses:* Carole Sousa: Department of Neurology and Neurophysiology, Freiburg  
20 University Medical Center; Annette Masuch: Anklam Extrakt GmbH, Johann-Friedrich-Böttger-Str.  
21 4, D-17389 Anklam; Simone Brioschi: Department of Pathology and Immunology, Washington  
22 University, St. Louis, MO 63110, USA; Ahmad Allouche: ETAP-Lab, Vandoeuvre-les-Nancy, F-  
23 54500, France; Nicolas Fischer: STROK@LLIANCE, Pôle de Recherche et innovation en Santé, F-  
24 14032 Caen, France; Knut Biber: AbbVie Pharmaceutical Research and Development, D-67061  
25 Ludwigshafen-am-Rhein, Germany

26

27 *Corresponding author:* Dr. Manuel Buttini- Luxembourg Centre for Systems biomedicine  
28 (LCSB), University of Luxembourg, 7, Avenue des Hauts Fourneaux, 4362 Esch-sur-Alzette,  
29 Luxembourg; Tel: 00352-4666-44-6183 ; Email: [manuel.buttini@uni.lu](mailto:manuel.buttini@uni.lu)

30

31 **Abstract**

32 A key process of neurodegeneration in Parkinson's disease (PD) is the transneuronal  
33 spreading of  $\alpha$ -synuclein. Alpha-synuclein is a presynaptic protein that is implicated in the  
34 pathogenesis of PD and other synucleinopathies, where it forms, upon intracellular  
35 aggregation, pathological inclusions. Other hallmarks of PD include neurodegeneration and  
36 microgliosis in susceptible brain regions. Whether it is primarily transneuronal spreading of  
37  $\alpha$ -synuclein particles, inclusion formation, or other mechanisms, such as inflammation, that  
38 cause neurodegeneration in PD is unclear. We used spreading/aggregation of  $\alpha$ -synuclein  
39 induced by intracerebral injection of  $\alpha$ -synuclein preformed fibrils into the mouse brain to  
40 address this question. We performed quantitative histological analysis for  $\alpha$ -synuclein  
41 inclusions, neurodegeneration, and microgliosis in different brain regions, and a gene  
42 expression profiling of the ventral midbrain, at two different timepoints after disease  
43 induction. We observed significant neurodegeneration and microgliosis in brain regions not  
44 only with, but also without  $\alpha$ -synuclein inclusions. We also observed prominent microgliosis  
45 in injured brain regions that did not correlate with neurodegeneration nor with inclusion load.  
46 In longitudinal gene expression profiling experiments, we observed early and unique  
47 alterations linked to microglial mediated inflammation that preceded neurodegeneration,  
48 indicating an active role of microglia in inducing neurodegeneration. Our observations  
49 indicate that  $\alpha$ -synuclein inclusion formation is not the major driver in the early phases of  
50 PD-like neurodegeneration, but that diffusible, oligomeric  $\alpha$ -synuclein species, which induce  
51 unusual microglial reactivity, play a key role in this process. Our findings uncover new  
52 features of  $\alpha$ -synuclein induced pathologies, in particular microgliosis, and point to the  
53 necessity of a broader view of the process of "prion-like spreading" of that protein.

54

55 **Key words:** alpha-synuclein spreading, neuroinflammation, Parkinson's disease,

56 microgliosis, transcriptional profiling, neurodegeneration

57

## 58 **Introduction**

59 Protein misfolding and aggregation are central pathological processes in neurodegenerative  
60 diseases, where they are believed to play a key role in driving the pathology [1, 2]. Proteins  
61 such as the amyloid beta peptide (A $\beta$ ) and tau in Alzheimer's disease (AD), TAR DNA-  
62 binding protein 43 (TDP43) in fronto-temporal dementia or motor neuron disease, prion in  
63 Creutzfeldt-Jakob disease, and finally alpha-synuclein ( $\alpha$ -syn) in Parkinson's disease (PD),  
64 are all examples of physiologically occurring proteins that, upon pathological misfolding,  
65 form oligomers, fibrils, and extracellular (A $\beta$ , prion) or intracellular (TDP43, tau,  $\alpha$ -syn)  
66 deposits, and injure neurons in the process [3-5].

67 An important property of these disease-associated proteins is their ability to self-  
68 propagate. This has been known for decades in prion diseases, in which disease-associated  
69 misfolding proteins themselves are sufficient to induce the disease process when transposed  
70 into a susceptible recipient host already decades ago [3, 6]. They do so by acting as a seed  
71 and corrupting the endogenous form of the protein, leading it to aggregate and form, over  
72 time, intracellular inclusions along interconnected neuronal pathways [7, 8]. Currently, the  
73 predominant narrative of this "spreading hypothesis" is that misfolded/aggregated particles of  
74 a disease protein move transsynaptically from neuron to neuron, causing dysfunction and  
75 damage along the way [4, 8]. Major support for this hypothesis comes from two observations.  
76 First, the neuropathological studies by Braak and colleagues, staging tau inclusions in AD  
77 [9], and Lewy inclusions in PD [10], suggest a progressive appearance, starting first in a  
78 population of susceptible neurons, of proteinaceous intraneuronal inclusions, a process that  
79 takes place over decades. Second, postmortem studies of in PD patients that had received  
80 intrastriatal fetal neuron transplants to combat dopamine loss, revealed Lewy bodies in a  
81 subset of the grafted neurons, indicating a spreading of abnormal  $\alpha$ -syn from the diseased  
82 neurons of the recipient to those of the donor [11, 12].

83           Alpha-syn is a presynaptic protein that normally is involved in the regulation of the  
84 synaptic vesicle cycle [13, 14]. Its involvement in PD was discovered when it was identified  
85 as an essential component of a PD pathological hallmark, the Lewy body [15], and when  
86 mutations in its gene, as well as dupli-or triplication thereof, were shown to lead to hereditary  
87 forms of the disease [16, 17]. Its prion-like spreading properties have been demonstrated in *in*  
88 *vitro* and *in vivo* model systems, using intracranial injection of Lewy-body containing brain  
89 extracts, of viral-construct mediated  $\alpha$ -syn overexpression and/or administration of pre-  
90 formed fibrils (PFFs) from recombinant  $\alpha$ -syn as seeds to induce spreading and  
91 aggregation[18] [19-22].

92           The role of  $\alpha$ -syn spreading and inclusion formation in PD pathogenesis is still unclear,  
93 since no correlation between PD symptoms and  $\alpha$ -syn inclusion load was consistently found  
94 [23-26]. Different possibilities that could explain what ultimately causes neuronal  
95 dysfunction and injury and, hence, neurological symptoms, have recently surfaced [27, 28].  
96 Among those, the notion that smaller moieties, or oligomers, of misfolded proteins rather  
97 than more fibrillar, deposited forms of  $\alpha$ -syn are the most neurotoxic has gained traction [29,  
98 30]. It is important to note that, in the field of AD, it was thought for decades that the A $\beta$   
99 deposited into plaques is the most harmful to neurons, whereas more recent evidence points  
100 to diffusible, soluble small A $\beta$  moieties as being the major neurotoxic form [31]. In the PD  
101 field though, this notion is still debated: while some studies report the potential harm  $\alpha$ -syn  
102 oligomers can cause [30, 32], other studies still contend that neuronal dysfunction and injury  
103 cannot occur without the demonstrable presence of inclusions [33, 34].

104           In this study, we addressed this issue by using a  $\alpha$ -syn seeding/spreading induced  
105 in wildtype mice [20]. We used intracranial administration of recombinant murine  $\alpha$ -syn  
106 PFFs to induce  $\alpha$ -syn spreading and inclusion formation in the brain of wildtype mice, and  
107 examined neurodegeneration and microgliosis in brain regions with  $\alpha$ -syn inclusions and,

108 importantly, in those without. We observed neurodegeneration in both cases, indicating that  
109 neuronal injury can occur independently of the progressive formation of  $\alpha$ -syn inclusions.  
110 Because neuroinflammation has emerged as a key player in neurodegenerative disease [35],  
111 and because microglia are the main cellular effectors of this process [36, 37], we also  
112 measured microgliosis in our model. We noticed, in regions with or without inclusions, a  
113 surprisingly strong microgliosis (4-5x over baseline), which far surpassed that observed after  
114 administration of neurotoxins such as the dopaminergic lesioning agent 6-hydroxydopamine  
115 (6-OHDA). In contrast to mice injected with 6-OHDA, neurodegeneration and microgliosis  
116 did not correlate with each other in the brains of  $\alpha$ -syn PFFs injected mice. Moreover, by  
117 measuring gene expression profiles after intrastriatal  $\alpha$ -syn PFF injection, we observed  
118 numerous significant changes in inflammation-related genes and pathways, and an unusual  
119 microglial molecular activation profile that preceded neuron loss and indicated a direct  
120 involvement of these cells in the neurodegeneration process.

121         These findings indicated that, in this model, microgliosis does not occur primarily as a  
122 response to neuronal damage, but is likely part of an intrinsic response to a process that is  
123 independent of the progression of  $\alpha$ -syn inclusion formation. Our results demonstrate that  
124 PD-like neurodegeneration can occur independently of the presence of  $\alpha$ -syn inclusions, and  
125 thus that PD-like pathologies is more than just the progressive formation of pathological  
126 inclusions. It may involve spreading of other, more soluble forms of toxic aggregates, such as  
127 oligomers, inducing an excessive microglial response, before inclusions are formed. We  
128 believe these results add an important aspect on how the pathogenic properties of “prion-like”  
129  $\alpha$ -syn should be viewed, and how future therapeutic interventions for PD will be designed.

130

## 131 **Materials and Methods**

132

133 *Expression, and purification of recombinant murine  $\alpha$ -Syn, and generation of pre-formed*  
134 *fibrils (PFFs), and of oligomers*

135 Expression and purification of recombinant murine  $\alpha$ -syn and generation of PFFs were  
136 performed as described [38]. PFFs were stored aliquoted at  $-80^{\circ}\text{C}$  until use. For the  
137 preparation of oligomers, recombinant  $\alpha$ -syn was purchased from Analytik Jena (Jena,  
138 Germany). Oligomers were generated as described [39, 40] by incubating soluble  $\alpha$ -syn in 10  
139 mM Tris-HCl, 100 mM NaCl under continuous shaking in an Eppendorf Thermomixer at  
140 650rpm and  $37^{\circ}\text{C}$  for 24 h, then stored aliquoted at 2 mg/ml at  $-80^{\circ}\text{C}$  until use.

141

142 *Western Blot of  $\alpha$ -syn PFFs and oligomers*

143 The composition of  $\alpha$ -syn PFFs and oligomers was checked by non-denaturing Western Blot.  
144 Three different concentrations of oligomers of PFFs (10 ng, 100 ng, 500 ng), were loaded on  
145 4-10% Precast Gel Mini Protean TGX (BioRad) according to manufacturer's instructions. To  
146 reveal  $\alpha$ -syn bands, anti-synuclein antibody clone 4D6 (Covance) was used at 1:2000 dilution  
147 (2 h at RT incubation), followed by IRDye<sup>R</sup> 800 CW donkey anti-mouse, diluted 1:10.000 (1  
148 h at RT incubation). Image was captured with a LI-COR Bioscience C-Digit  
149 Chemoluminescence scanner.

150

151 *Animals*

152 Three- to 6- month-old C57Bl/6J mice were purchased from Jackson via Charles River (Bois-  
153 des-Oncins, France), or Janvier Labs (Le-Genet-St.-Isle, France). Mice were housed in  
154 individually -ventilated cages (IVC) in a conventional animal facility of the University of  
155 Luxembourg, or in the facility of SynAging, in Vandoeuvre-les-Nancy, France. All animal  
156 studies were in agreement with the requirements of the EU Directive 2010/63/EU and  
157 Commission recommendation 2007/526/EC. Male or female mice were housed under a 12h-

158 12h dark/light cycle with *ad libitum* access to water and food (#2016, Harlan, Horst, NL). For  
159 time point of 90 dpi PFF injections (see below), the youngest mice were used, for time point  
160 13 dpi PFF injections, the oldest mice were used, so that, at euthanasia, all the mice were of  
161 comparable age (6 to 6.5 months). Otherwise, mice were assigned randomly to study groups.  
162 For quantitative histology (see below), 10-11 mice/group were used, and all were quantified,  
163 whereas for transcriptional profiling, 6 mice/group were used. Such numbers have proven  
164 sufficient in previous studies on different models of neurodegeneration, while also keeping in  
165 line with the rule of the “3Rs” [41-45]. Animal studies were approved by the institutional  
166 Animal Experimentation Ethics Committee of the University of Luxembourg and the  
167 responsible Luxembourg government authorities (Ministry of Health, Ministry of  
168 Agriculture). Alternatively, experiments done at the SynAging site were approved by ethics  
169 committee “Comité d’Ethique Lorrain en Matière d’Expérimentation Animale”, and by the  
170 governmental agency the “Direction Départementale de la Protection des Populations de  
171 Meurthe et Moselle- Domaine Expérimentation Animale”.

#### 172 *Intrastriatal injections of $\alpha$ -syn PFFs, $\alpha$ -syn oligomers, and 6-hydroxydopamine*

173 Alpha-syn PFFs were sonicated in a sonicating waterbath (Branson 2510, Danbury, CT) for 2  
174 hours at RT, keeping the temperature constant at 25°C by adding ice as needed, or using the  
175 Bioruptor UCD 300 (Diagenode, Seraing, Belgium) with 30 cycles of 15sec ON/ 15sec OFF  
176 at 4°C. Sonicated PFFs were kept on ice and used within ten hours. Mice were injected under  
177 isoflurane anesthesia (2%) on a heating pad. A 1 cm long mid-line scalp incision was made  
178 into the disinfected surgical area and a 0.5 mm hole drilled unilaterally into the skull using  
179 stereotaxic coordinates for striatum according to the Mouse Brain Atlas of Franklin and  
180 Paxinos [46]. Ten  $\mu$ g of PFFs, or respective PBS solution (control mice) were administered,  
181 in volumes of 2  $\mu$ l, within the right dorsal striatum at the following relative-to-bregma  
182 coordinates: anterior +0.5 mm, lateral +2.1 mm; depth +3.2 mm. The 24-gauge blunt tip



183 needle of the Hamilton syringe (7105KH, Bonaduz, CH) was inserted down 3.3 mm for 10  
184 seconds to form an injection pocket, and the needle remained in place for 2 minutes before  
185 and after the injection procedure. The hole was covered with bonewax (Lukens, Arlington,  
186 VA) and the wound closed using 7mm Reflex wound clips (Fine Science Tools, Heidelberg,  
187 Germany). Two % xylocaine gel was applied to the wound, and mice were allowed to recover  
188 from anesthesia before being put back into their home cages. The day of injection of PFFs  
189 was named day 0. Same coordinates and similar procedure were used for 6-OHDA or  $\alpha$ -syn  
190 oligomers. Striatal injection of 6-OHDA has been described elsewhere [47]. Striatal  
191 injections of  $\alpha$ -syn oligomers were done with 4  $\mu$ g oligomers in 2  $\mu$ l vehicle. Control mice  
192 received the same volume of vehicle (see above). Mice were euthanized in a deep anaesthesia  
193 (i.p. injection of Medetomidin, 1mg/kg and Ketamin, 100mg/kg) by transcardial transfusion  
194 with PBS. PFF-injected mice were euthanized either at day 13 (13 dpi) or at day 90 (90 dpi)  
195 after intrastriatal injections (“day 0”: day of injection). Mice injected with oligomers or with  
196 6-OHDA were euthanised at 13 dpi.

197

#### 198 *Tissue extraction and preparation*

199 For immunohistochemistry, extracted brains were fixed in in 4% buffered PFA for 48h and  
200 kept in PBS with 0.1% NaN<sub>3</sub> until they were cut with a vibratome (VT1000 S from Leica)  
201 into sagittal 50 $\mu$ m free-floating sections. Before the staining procedure, sections were kept at  
202 -20°C in a cryoprotectant medium (1:1 v/v PBS/Ethylene Glycol, 10g.L<sup>-1</sup> Polyvinyl  
203 Pyrrolidone). Alternatively, for dopamine measurement or RNA extraction, after removal  
204 from the skull, brains were dissected on ice into regions, and isolated striatum and ventral  
205 midbrain were quickly weighted, then snap-frozen on dry ice until further processing.  
206 Extraction and measurement of striatal dopamine (DA) has been described elsewhere [48].  
207 Briefly, after homogenization and derivatization, striatal metabolites were measured with a

208 gas-chromatography/mass-spectrometry set-up (Agilent 7890B GC – Agilent 5977A MSD,  
209 Santa Clara, CA). Absolute level of DA were determined using an internal standard, 2-(3,4-  
210 Dihydroxyphenyl)ethyl-1,1,2,2-d<sub>4</sub>-amine HCl (D-1540, C/D/N isotopes, Pointe-Claire,  
211 Canada). For RNA extraction from the ventral midbrain, the RNEasy Universal Kit  
212 (Quiagen) was used, after homogenization of midbrain tissues in a Retsch MM 400 device (2  
213 min at 22Hz, Haan, Germany). RNA concentrations and integrity were determined using a  
214 Nanodrop 2000c (Thermo Scientific) and a BioAnalyzer 2100 (Agilent), respectively.  
215 Purified RNAs were considered of sufficient quality if their RNA Integrity Number (RIN)  
216 was above 8.5, their 260/230 absorbance ratio > 1, and their 260/280 absorbance ratio = 2.

217

#### 218 *Single and double-label immunohistochemistry*

219 Immunostaining procures followed standard protocols, as described [41, 42]. All stainings,  
220 except those for proteinase-K resistant  $\alpha$ -syn inclusions (see below), were performed on free-  
221 floating 50  $\mu$ m-thick sections. Supplemental Table 1 lists all primary and secondary  
222 antibodies used in this study, as well as their dilutions. All other reagents were from Sigma  
223 unless indicated otherwise. All antibody incubations were at room temperature, except for the  
224 anti-synaptophysin antibody, which was incubated at 4°C. Sections were washed 3 x in PBS  
225 between each incubation step. To block endogenous peroxidases and for permeabilization,  
226 sections were incubated with 3% H<sub>2</sub>O<sub>2</sub> v/v and 1.5% Triton X100 v/v for 30 min. For  
227 immoperoxidase staining with anti-synuclein antibody, this step was followed by an epitope  
228 unmasking step with 75% v/v formic acid for 5 min. To avoid unspecific antibody binding,  
229 sections were incubated with 5% serum (Vector Laboratories, Burlingame, CA) or 5% BSA  
230 w/v in PBS for 1h before they were incubated with the respective primary antibody, or  
231 antibodies in case of double labeling. The following day, sections were incubated with a  
232 secondary antibody for 1-2 hours (fluorophore-coupled for immunofluorescence, or

233 biotinylated for immunoperoxidase). Singly or doubly fluorescently-stained sections were  
234 mounted on Superfrost plus slides (Thermoscientific, Walham, MA), air-dried, and  
235 coverslipped using ProLong Gold antifade mountant (Life technologies, Darmstadt,  
236 Germany). For immunoperoxidase staining, antibody binding was visualized using an ABC  
237 Vectastain Kit (Vector Laboratories), followed by detection with diaminobenzidine (Merck)  
238 and H<sub>2</sub>O<sub>2</sub> as peroxidase substrates. Sections were mounted, dried overnight and coverslipped  
239 with Neo-mount (Merck) after soaking in Neo-clear xylene substitute (Merck) for 10 min.  
240 Visualization of Proteinase-K resistant  $\alpha$ -synuclein inclusions was done by paraffin-  
241 embedded tissue blot (PET blot) on 3 $\mu$ m paraffin sections mounted on nitrocellulose  
242 membrane (0.45 $\mu$ m, BioRad) as previously [49].

243

#### 244 *Proximity ligation assay*

245 Protocol for PLA was adapted to be performed on free floating sections. All reactants were  
246 prepared according manufacturer's recommendations (Duolink. Sigma) and incubation times  
247 were as described [50]. Washes were performed in 24- well plates at RT, and reactions  
248 volumes were 40 $\mu$ L at 37°C. First, 20 $\mu$ g of anti-pSER129-  $\alpha$ -syn mouse monoclonal 11E5  
249 antibody (Prothena Biosciences, see suppl. table 1) were conjugated with either plus or minus  
250 oligonucleotide probes according manufacturer's recommendations, and stored 4°C until use.  
251 Free floating sections were washed in PBS and permeabilized as described above. Blocking  
252 was performed with DuoLink blocking solution for 2h RT. Sections were incubated overnight  
253 with both plus and minus probe-linked antibody (1:1 1/750 in Duolink antibody diluent  
254 solution). For ligation of the probes, after washing of the probe-linked antibodies (2 X 5min  
255 in Duolink's Buffer A), the ligation-ligase solution was added and incubated for 30 min at  
256 37°C. For detection, after washing of the ligation-ligase solution (2 X 5min in Duolink's  
257 Buffer A), sections were incubated with the amplification-polymerase solution for 2.5h at

258 37°C. Sections were then washed in Buffer B for ten minutes, and in Buffer B 0.01X for one  
259 minute prior mounting, dried in the dark, and coverslipped. Z-stacks of pictures were  
260 acquired at 40X with a Zeiss LabA1 microscope, a maximum intensity projection was created  
261 using the Zen Blue 2012 software (Zeiss).

262

### 263 *Quantitative neuropathology on immunostained sections*

264 Imaging of peroxidase- labelled sections for pSER129- $\alpha$ -syn, and of fluorescently labelled  
265 sections for Tyrosine-Hydroxylase (TH), Dopamine Transporter (DAT), or Ionized calcium  
266 binding adaptor molecule 1 (Iba1), was done on a Zeiss LabA1 microscope, coupled to a  
267 Zeiss AxioCam MRm3 digital camera, and to a PC using the Zeiss Zen Blue 2012 software.

268 Alpha-syn inclusions were visualized by immunostaining for pSER129- $\alpha$ -syn. For the  
269 quantitation of  $\alpha$ -syn inclusions in the frontal cortex and the amygdala (basolateral nucleus),  
270 2 immunoperoxidase labeled (see above) sections/animal were imaged, using the 10x  
271 objective (frontal cortex) or the 20x objective (amygdala). A total of 4-6 images were  
272 collected for each region (10x objective, 2 x 1.52 mm each image), and digitized. After  
273 manually drawing regions of interests and thresholding, the percent image area occupied by  
274 immunopositive structures was determined using the ImageJ v. 1.45 (NIH, Bethesda, MD)  
275 public domain software. All values obtained from sections of the same animal were averaged.

276 For the quantitation of  $\alpha$ -syn inclusions in the SN, double immunostainings for TH and  
277 pSER129- $\alpha$ -syn were performed. TH staining was used to locate the SN, and images were  
278 acquired at 10x magnification. Percent overlap of pSER129-  $\alpha$ -syn signal within the TH  
279 immunopositive area was calculated using ImageJ. For the quantitation of synaptophysin-  
280 positive synaptic terminals, fluorescently stained sections from each animal were viewed by a  
281 Zeiss LSM 710 laser-scanning confocal microscope, using a 20 $\times$  objective and a software  
282 magnification zoom factor was used to obtain images of 180  $\times$  180  $\mu$ m each. For each animal,

283 a total of 4-6 images were collected from the frontal cortex, and 4 from the hippocampal  
284 pyramidal region. Images were then transferred to a PC personal computer, and average  
285 intensity of positive presynaptic terminals was quantified for each image using the ImageJ.  
286 Values from individual animals were averaged. This method to quantify synaptic integrity  
287 has been validated by electron microscope quantitation of synaptic densities in a previous  
288 study [41].

289 The quantitation of degeneration of TH positive neurons in the SN has been described, and  
290 results obtained with this approach have been shown to correlate with stereological cell  
291 counts (supplemental material in Ashrafi et al. (2017) [47]). For the quantitation of striatal  
292 TH-positive neuronal fibers and of DAT-positive synaptic terminal, doubly labelled sections  
293 with anti-TH and anti-DAT were used. A total of six to nine 40x pictures (223.8 x 167.7  $\mu$ m  
294 each) of the dorsal striatum, from 2-3 sections per mouse, were acquired using the optical  
295 sectioning system Apotome.2 (Zeiss). The percent area occupied by TH and DAT was  
296 determined using Image J software and averaged for each mouse.

297 For the quantitation of microglial activation in the hippocampus and frontal cortex, 2 sections  
298 /animal were labeled for the microglial marker *Iba1*. For the frontal cortex, a total of 6, and,  
299 for the hippocampus, a total of 3-4 images were collected with a 40x objective (223.8 x 167.7  
300  $\mu$ m each image). Digitized images were transferred to a laptop computer, and, with ImageJ v.  
301 1.45, after thresholding, average area occupied by *Iba1*-positive microglia was measured. All  
302 values obtained from sections of the same animal were averaged. For the quantitation of the  
303 microglial activation in the SN, TH and *Iba1*- double-labeled sections were imaged with a  
304 10x objective. Average area covered by TH-positive neurons in control mice was used to  
305 determine the region of interest, restricted to the SN, to measure microglial activation. Four  
306 subregions of the SN were imaged and quantified for each mouse [47]. *Iba1* immunopositive  
307 cells were quantified within each subregions, averaged for each of them, and converted in

308 mm<sup>2</sup>. For each mouse, the sum of the four averaged subregions was used as a measure for  
309 microglial activation.

310 All quantitative neuropathological analyses were performed blinded on coded sections, and,  
311 for each of the measurements, codes were only broken when quantification for that measure  
312 in all animals was complete. For all measures, the ipsilateral and contralateral values of PBS-  
313 injected control mice were similar (no statistical difference detected), these values were  
314 grouped. Statistics on quantitative histological data were done using the GraphPad Prism 8  
315 software. ANOVA followed by Dunnett's post-hoc was used for normally distributed data  
316 sets. Pearson's test, or Spearman's rank test where appropriate, were used to study linear  
317 correlations. P values smaller than 5% were considered as significant.

318

#### 319 *Microarray analysis and calculation of differentially expressed genes*

320 GeneChip Mouse Gene 2.0ST Arrays (Affymetrix) were used for transcriptional profiling.  
321 Total RNAs (150ng) were processed using the Affymetrix GeneChip® WT PLUS Reagent  
322 Kit according to the manufacturer's instructions (Manual Target Preparation for GeneChip®  
323 Whole Transcript (WT) Expression Arrays P/N 703174 Rev. 2). In this procedure, adapted  
324 from Bougnaud et al. (2016) [51], the purified, sense-strand cDNA is fragmented by uracil-  
325 DNA glycosylase (UDG) and apurinic/aprimidinic endonuclease 1 (APE 1) at the unnatural  
326 dUTP residues and breaks the DNA strand. The fragmented cDNA was labelled by terminal  
327 deoxynucleotidyl transferase (TdT) using the Affymetrix proprietary DNA Labelling Reagent  
328 that is covalently linked to biotin; 5.5 µg of single-stranded cDNA are required for  
329 fragmentation and labelling, then 3.5 µg of labeled DNA + hybridization controls were  
330 injected into an Affymetrix cartridge. Microarrays were then incubated in the Affymetrix  
331 Oven with rotation at 60 rpm for 16 hr at 45°C, then the arrays were washed and scanned  
332 with the Affymetrix® GeneChip® Scanner 3000, based on the following protocol:

333 UserGuide GeneChip® Expression Wash, Stain and Scan for Cartridge Arrays P/N 702731  
334 Rev. 4, which generated the Affymetrix raw data CEL files containing hybridization raw  
335 signal intensities were imported into the Partek GS software. First, probe intensities were  
336 summarized to gene expression signals using Partek default options (GCcontent adjustment,  
337 RMA background correction, quantile normalization, log<sub>2</sub> transformation and summarization  
338 by means).

339 For statistical analysis, the normalized and log<sub>2</sub> transformed data was loaded into the  
340 R/Bioconductor statistical environment. The rank product (Package: **RankProd**) approach  
341 was chosen to determine the differentially expressed genes (DEGs) [52-54]. Rank product  
342 statistics were computed, since they have been shown to enable a robust non-parametric  
343 analysis of microarray datasets with limited number of samples [52]. Estimated p-values and  
344 pfp (percentage of false prediction) values were determined and used as nominal and  
345 adjusted significance scores, respectively. Pfp scores estimate the significance of differential  
346 expression after adjusting for multiple hypothesis testing, and can have values larger than 1.  
347 The chosen significance cut-offs were p-value < 0.05 and pfp < 0.1. A relaxed cut-off (pfp <  
348 0.1 instead of < 0.05) was chosen to avoid loss of information for the subsequent enrichment  
349 analysis, which combines several genes below this threshold to enable detection of pathway  
350 alterations. No minimal fold change threshold was applied.

351 For visualization of differential gene expression, Venn diagrams and heatmaps were  
352 generated using the **VennDiagram** and **gplots** packages, respectively, in R. Data pre-  
353 processing included removal of all transcripts missing gene IDs and duplicated entries (after  
354 ranking). To avoid mismatches or other discrepancies, the Affymetrix probe sets IDs were  
355 used to calculate the overlapping DEGs between the different comparisons. Diagrams were  
356 generated for the following criteria and comparisons: 1) 13 dpi & 90 dpi - ipsiPFF *versus*  
357 ipsiPBS (p-value < 0.05); 2) 13 dpi & 90 dpi – ipsiPFF *versus* ipsiPBS (pfp < 0.1); 3) 13 dpi

358 & 90 dpi - ipsiPFF *versus* contraPFF (p-value < 0.05); 4) 13 dpi & 90 dpi – ipsiPFF vs  
359 contraPFF (pfp < 0.1). In a second step, we were interested in investigating the expression  
360 direction of the overlapping transcripts between the early to late timepoint. Therefore, we  
361 extracted the probe IDs, matched the individual lists and grouped them into high and low  
362 expressed transcripts. Then, the above mentioned venn diagrams were generated with these  
363 newly generated lists. Heatmaps were generated using the *heatmap.2* function for ipsiPFF vs  
364 ipsiPBS and ipsiPFF vs contraPFF for p-value < 0.05 and pfp < 0.1 at 13 dpi and 90 dpi  
365 respectively. The log<sub>2</sub>-transformed data matrix was used to plot. Additionally, we applied  
366 hierarchical top down clustering (*cor* and *hclust* basic R functions) and the data matrix was  
367 scaled row-by-row generating Z-scores.

368

#### 369 *Gene Set Enrichment Analysis*

370 The enrichment analysis for GO terms (biological processes (BP) only) was performed using  
371 the GUI (graphical user interface) version GSEA (version 3.0) published by the Broad  
372 Institute (download: <http://software.broadinstitute.org/gsea/downloads.jsp>) [55]. All  
373 parameters were set to default in GSEA, except “Collapse dataset to gene symbols” was set to  
374 “false”, “Permutation type” was set to “gene\_set” and “Max size: excluding larger sets” was  
375 set to “250”. One optimization step was introduced: a customized GMT/GMX file was  
376 generated in R/Bioconductor with mouse NCBI EntryzIDs as gene identifiers. This file was  
377 used as the “Gene sets database” in GSEA. The resulting enrichment scores (ES) were  
378 obtained applying the weighted Kolmogorov-Smirnov-like statistics. ES reflect the level to  
379 which a gene set is overrepresented among the top up- or down-regulated genes in a ranked  
380 gene list, then, the ES statistic was normalized (normalized enrichment scores, NES) as  
381 described [55]. Finally, the p-value significance scores were adjusted for multiple hypothesis  
382 testing using the method by Benjamini and Hochberg[56] to provide final FDR scores. A



383 network map of the enrichment analysis results was generated using Cytoscape [57]. The  
384 mapping parameters used in Cytoscape were: p-value < 0.05, FDR Q-value < 0.1 (default  
385 setting is 1) and Overlap > 0.5. The enrichment map was automatically launched from GSEA  
386 and created in Cytoscape. In the enrichment maps, nodes represent enriched gene sets  
387 associated with BPs, and edges the degree of similarity between them using the overlap  
388 coefficient (threshold > 0.5). Further curation of gene sets was done manually. Since gene  
389 sets with similar gene compositions tend to group together, such gene set clusters were easily  
390 identifiable. Nodes grouped into more than one gene cluster according to this procedure were  
391 assigned to the most overlapping cluster, i.e. the cluster they were associated with by a  
392 shorter sequence of connecting edges in the ontology graph. All softwares used are listed in  
393 Supplemental table 2.

394

#### 395 *Identification of cellular source of DEGs*

396 For the identification of the cellular source of specific DEGs, the public database  
397 <https://www.brainrnaseq.org/> was used.

398

## 399 **Results**

400

### 401 **Western blot characterisation of $\alpha$ -syn moieties**

402 A non-denaturing blot of the  $\alpha$ -syn moieties used in this study is shown in supplemental Fig,  
403 1. For intrastriatal injections,  $\alpha$ -syn oligomers were used non-sonicated, whereas  $\alpha$ -syn PFFs  
404 were sonicated. Based on their profile on WB, the oligomer preparation was composed  
405 mainly of monomers, dimers, and trimers, as well as higher molecular weight species. The  
406 sonicated PFFs were composed mainly of monomers and dimers, and higher molecular  
407 weight species. When compared to their non-sonicated counterparts, sonicated PFFs seemed

408 to have less of all these components, consistent with a shearing effect of sonication that  
409 produces smaller  $\alpha$ -syn fragments, which may then act as seeds.

410

#### 411 **Intrastriatal injection of PFFs causes bilateral $\alpha$ -syn inclusions in multiple brain regions**

412 Because we wanted to capture the early features of  $\alpha$ -syn spreading associated pathologies,  
413 we decided to focus our investigations on time points when, these pathologies have not  
414 reached a peak yet [20]. Since  $\alpha$ -syn inclusions have been suggested to be a major driver of  
415 PD-like pathology [34, 58], we first looked at the appearance of these inclusions in our  
416 model.

417 To determine if intrastriatal injection of murine  $\alpha$ -syn PFF reliably induced propagation of  
418 fibrillar  $\alpha$ -syn in our mice, we first performed immunohistochemistry against pSER129-  $\alpha$ -  
419 syn on sections of both brain hemispheres 13 days and 90 days after they had been injected  
420 with PFFs (13 dpi, 90 dpi). Immunostaining for pSER129-  $\alpha$ -syn is the most commonly used  
421 approach to detect  $\alpha$ -syn inclusions in rodent or human brain tissues [59].

422 At an early time point after  $\alpha$ -syn PFF administration (13 dpi), we only detected few  
423 pSER129-  $\alpha$ -syn positive inclusions in frontal cortex, amygdala, and SN, and more in the  
424 ipsilateral striatum (supplemental Fig. 2).

425 However, at 90dpi, we observed robust appearance of pSER129-  $\alpha$ -syn positive cellular and  
426 neuritic inclusions in the ipsi- and contralaterally, in the same brain regions (Fig.1 A).  
427 Quantitation of image area occupied revealed median coverage of 10% for the ipsilateral  
428 frontal cortex, 5% for the contralateral frontal cortex, 8% for the ipsilateral amygdala, 4.2%  
429 for the contralateral amygdala, and 12% for the ipsilateral SN. No or very few  $\alpha$ -syn  
430 inclusions were found in the contralateral SN and striatum, and no inclusions in either side of  
431 the hippocampus. Cells containing inclusions had neuronal morphology. In the ipsilateral SN,

432 fluorescent double staining for pSER129- $\alpha$ -syn and TH, a marker for dopaminergic neurons  
433 in the SN, showed that 85% of inclusions co-localized with TH-positive neurons, indicating  
434 that most, if not all, inclusions are localized in neurons.

435 To determine if the pSER129-  $\alpha$ -syn positive inclusions were Proteinase-K resistant , we  
436 performed a Proteinase-K assay PET assay [49]. We observed numerous pSER129-  $\alpha$ -syn  
437 positive signals in these tissue sections (Fig. 1 B), indicating that most inclusions were  
438 proteinase-K resistant.

439 Inclusions are not the only  $\alpha$ -syn species that have been suggested to be linked to  
440 neurodegeneration in PD. To determine if regions without detectable  $\alpha$ -syn inclusions, such  
441 as the hippocampus, were still affected by abnormal  $\alpha$ -syn after injection of PFFs, we  
442 performed a Proximity Ligation Assay (PLA). This assay has been used for detecting  
443 oligomeric forms of  $\alpha$ -syn in human [60] and mouse models of PD [61]. We observed greatly  
444 enhanced signal intensity in the hippocampi of PFF-injected mice than in those of control  
445 mice (Fig. 1C), indicating the presence of abnormal levels of oligomeric  $\alpha$ -syn in that area.

446 Overall, the pattern of  $\alpha$ -syn inclusions we observed 90 dpi matches that described at a  
447 similar time point by Luk et al. (2012) [20]. The robust appearance of intracellular  $\alpha$ -syn  
448 inclusions in this model opened up the possibility of analyzing how they are associated with  
449 other pathological hallmarks, such as neurodegeneration and –inflammation, and which of  
450 these events might precede the others.

451

#### 452 **Intrastriatal injection of PFFs causes bilateral synaptic loss and unilateral** 453 **dopaminergic neuron injury that is independent of $\alpha$ -syn inclusions**

454 We set out to determine to what extent the presence of neuronal  $\alpha$ -syn deposition was linked  
455 to neurodegeneration, 90 dpi after intrastriatal administration of PFFs.

456 First, we analyzed synaptic degeneration in the hippocampus and frontal cortex. In these  
457 brain regions, we measured the level of the presynaptic protein synaptophysin.  
458 Synaptophysin is a good marker for synaptic integrity [41, 62, 63], and pathological synaptic  
459 alterations have been reported in PD post-mortem tissues [64]. Roughly 60% of PD patients  
460 suffer from cognitive impairments and dementia [65], indicating that their hippocampus, as a  
461 major region involved in memory formation, and their higher cortical association areas are  
462 affected. Finally, *in vitro*, addition to PFFs to cultured primary hippocampal neurons was  
463 reported to affect these neuron's synaptic integrity and function [66]. Thus, we measured  
464 synaptophysin ipsi- and contralaterally in these brain regions in mice 90 dpi after PFF  
465 administration (Fig. 2). We found, in both regions, a highly significant, bilateral 20-25%  
466 reduction of this protein. Interestingly, we noticed this decrease in the absence of  $\alpha$ -syn  
467 inclusions in the hippocampus. The  $\alpha$ -syn oligomers though (Fig. 1) in that region may be  
468 linked to synaptophysin loss.

469 Next, we examined the SN, because it contains dopaminergic neurons that are one of the  
470 most susceptible to PD-associated disease challenges. We measured the area occupied by  
471 tyrosine hydroxylase (TH)-positive neuronal profiles in the SN ipsilaterally, where  $\alpha$ -syn  
472 inclusions were present (see above), but also contralaterally, which was without such  
473 inclusions. We did not find any sign of degeneration in the striatum or SN at 13 dpi  
474 (Supplemental fig. 2). We found though a 16% decrease of TH-positive neurons in the  
475 ipsilateral SN, that was significant, but not in the contralateral SN (Fig 2). To determine if  
476 striatal axonal projections of dopaminergic neurons were affected in our model, we analyzed  
477 the morphological integrity of these projections and their synaptic terminals. We observed, 90  
478 dpi, a significant decrease in TH-positive axonal fibers as well as in dopamine transporter  
479 (DAT) positive synaptic terminals, in the ipsilateral, but not the contralateral striatum. To  
480 confirm ipsilateral striatal injury, we measured the neurotransmitter dopamine (DA) in

481 dissected ipsi- and contralateral striata of PFF-injected and PBS control mice (n=8-12/group).  
482 We found a significant decrease in ipsilateral striatum of PFF mice compared their ipsilateral  
483 PBS controls (19.5+/-5.8 versus 27.5+/-7.3 pmol/mg; p=0.02 by ANOVA followed by  
484 Sidak's posthoc, results are means +/- S.D.), but no difference between contralateral striatum  
485 of PFF mice compared to their compared their ipsilateral PBS controls (27.3+/-3.7 pmol/mg  
486 versus 28.5+/-5.7 pmol/mg). This conformed our histological observations.

487

488 **Widespread, pronounced, and bilateral microgliosis, caused by intrastriatal injection of**  
489  **$\alpha$ -syn fibrils.**

490 Microglia, the local CNS innate immune defense cells [67], react rapidly to CNS infection or  
491 injury in an orchestrated fashion. Functional imbalances of these cells can precipitate disease  
492 outcomes [36, 37, 68]. While strong microgliosis has been reported in PD and models thereof  
493 [69-71], the role of these cells in disease initiation and progression of PD is poorly  
494 understood.

495 To better understand the role of these cells in the context of  $\alpha$ -syn spreading, and more  
496 precisely to determine if they have a role in driving the neurodegeneration we observed, we  
497 first analysed their response using a specific marker (Iba1), in mouse brains after injection of  
498  $\alpha$ -syn PFFs. We observed a surprisingly strong (4-5 times over control in some brain  
499 regions), microgliosis in brain regions with (bilaterally in frontal cortex, amygdala, SN) at 90  
500 dpi. The microgliosis was present in brain regions with inclusions, but also those without  
501 (hippocampus) or very little (contralateral SN) inclusions (Fig. 3). While no significant Iba1  
502 increase was seen at 90 dpi in the ipsilateral striatum in PFF injected mice, microglial  
503 Cluster-of-Differentiation 68 (CD68), a marker for phagocytic activity, was increased. No  
504 significant microgliosis was observed at 13 dpi (Supplemental fig. 2). Microglia in PFF-  
505 injected mice had thickened, though still ramified, processes, and an intensely stained cell

506 soma. In the cerebellum, which was devoid of  $\alpha$ -syn deposits in all mice, we could not detect  
507 any differences in Iba1 positive microglia between PFF-injected and control PBS injected  
508 mice (not shown).

509 Our observations indicate that a robust, widespread microglial reaction is an important part of  
510 the  $\alpha$ -syn spreading process, and warranted further investigation into the pathological  
511 implications of that reaction.

512

513 **Neurodegeneration and microgliosis neither correlated with  $\alpha$ -syn deposition, nor with**  
514 **each other.**

515 To gain insight into the pathological properties of  $\alpha$ -syn inclusions, we correlated the  
516 inclusion load with neurodegeneration and with microgliosis measured locally in frontal  
517 cortex and SN. We found that inclusion load correlated with neither of the two (Fig. 4). Thus,  
518 neurodegeneration as well as microgliosis induced by  $\alpha$ -syn PFFs were independent of  $\alpha$ -syn  
519 deposition.

520 The strong microgliosis in different brain regions after administration of PFFs prompted us to  
521 look into this observation further. In the brain, microglia react rapidly to tissue injury to  
522 control the damage and clear up cell debris [37, 72]. Thus, microglial reaction is typically  
523 secondary to an underlying neurodegenerative process, and, as a consequence, increase of  
524 microglial reaction is directly associated with increase in neuronal damage. For instance, we  
525 have observed that microglial reaction (measured on Iba1 immunostained sections) correlated  
526 with TH neuron loss in the ipsilateral SN after unilateral 6-OHDA lesioning (Fig. 4B2), and  
527 with synapse or dendritic loss in the cortex after lesioning with the excitotoxin kainic acid  
528 [43]. After intracerebral injection of  $\alpha$ -syn PFF though, we found that microglial reaction was  
529 not only much stronger than after injection of neurotoxins (4-5x *versus* 2-3x over control),

530 but also failed to correlate with measures of neurodegeneration (TH neuron loss in the SN,  
531 synaptophysin in the cortex and hippocampus) (Fig. 4B). This observation indicates that the  
532 microglial reaction to  $\alpha$ -syn spreading may be a direct response to factors produced during  
533 that process, and not just a secondary response to neuronal degeneration, as is the case after  
534 injection of neurotoxins.

535

536 **Microglia across several brain regions react strongly to intrastriatal injection of  $\alpha$ -syn**  
537 **oligomers**

538 Several studies have indicated that microglia are activated *in vitro* by  $\alpha$ -syn oligomers [73,  
539 74]. As described above, we have observed the presence of  $\alpha$ -syn oligomers, notably in the  
540 hippocampus, after intrastriatal injection of  $\alpha$ -syn PFFs. To test whether  $\alpha$ -syn oligomers  
541 could be the factor that leads to a strong microglial reaction during the  $\alpha$ -syn spreading  
542 process, we injected such oligomers into the same location as the PFFs, the dorsal striatum.  
543 Just 13 dpi, we observed, on Iba1 stained sections, a strong microglial reaction in the  
544 ipsilateral striatum, frontal cortex, and hippocampus (Fig. 5). Qualitatively, the reaction was  
545 even stronger than 90 dpi after PFF injection. This observation shows that, in a mouse brain,  
546  $\alpha$ -syn oligomers can induce a microglial reaction, even at a distance from the injection site.  
547 Thus,  $\alpha$ -syn oligomers emerge as the likely factor that, by diffusing through the brain,  
548 induces a strong microglial reaction during the process of  $\alpha$ -syn spreading.

549

550 **Transcriptional profiling of ventral midbrain reveals most gene expression changes**  
551 **occur 13 days after  $\alpha$ -syn PFF injection**

552 To investigate the molecular underpinnings of the neurodegeneration and of the microglial  
553 response accompanying  $\alpha$ -syn spreading, we generated a gene expression profile from  
554 ventral midbrain of PFF injected and control mice using the Affymetrix gene expression  
555 profiling platform. Because microglial response typically starts early after an insult [67, 75],  
556 we analyzed the midbrain gene expression profiles 13 dpi (no neurodegeneration) and 90 dpi  
557 (neurodegeneration in the ipsilateral striatum and midbrain) after intrastriatal  $\alpha$ -syn PFF  
558 injection.

559 We focused on two comparisons of ventral midbrain gene expression profiles: 1. ipsilateral  
560 midbrain of PFF-injected mice (ipsi PFF, with degeneration of nigral TH neurons and their  
561 striatal projections) *versus* ipsilateral midbrain of control PBS-injected mice (ipsi PBS), 2.  
562 ipsilateral midbrain of PFF-injected mice *versus* contralateral midbrain of the same, PFF-  
563 injected, mice (contra PFF, without loss of nigral TH neurons and their striatal projections).  
564 We figured that these two comparisons would be best suited to reveal relevant gene  
565 expression changes.

566 The number of DEGs that emerged in these comparisons, and the number of overlapping  
567 DEGs between the two time points (13 dpi and 90 dpi) are shown in Fig. 6. By comparing  
568 ipsi PFF to ipsi PBS, applying a cut-off of  $p < 0.05$ , we found a total of 2.631 significant DEG  
569 at 13 dpi, and significant 2584 DEG at 90 dpi, with 985 overlapping DEGs between the two  
570 time points. After correcting for multiple hypothesis testing at a cut-off of  $p < 0.1$ , we  
571 found 266 DEGs at 13 dpi, and 82 DEGs at 90 dpi, with 39 DEGs overlapping between the  
572 two times points. The majority of overlapping DEGs showed upregulation at 13 dpi, but  
573 downregulation at 90 dpi (Venn diagrams of overlapping DEGs in Fig. 7), indicating active  
574 gene expression at the early time point after PFF injection. By comparing ipsi PFF to contra  
575 PFF, we found 3.477 significantly DEGs at 13 dpi, and 3.209 DEGs at 90 dpi, with 1356  
576 overlapping DEGs between the two time points. At  $p < 0.1$ , we found 648 DEGs at 13 dpi,



577 and 588 DEGs at 90 dpi, with 227 overlapping DEGs. At 13 dpi, we found a similar number  
578 of upregulated *versus* downregulated DEGs, but at 90 dpi, we saw that most DEGs were,  
579 interestingly, downregulated.

580 Taken together, these two comparisons indicate that enhanced gene expression changes  
581 occurred in the ventral midbrains of both hemispheres at 13 dpi, probably setting the stage for  
582 the subsequent pathological events. In contrast, at 90 dpi, in the ipsilateral midbrain, most  
583 DEGs dial their expression level back, indicating a reduction in gene transcription, while the  
584 major pathological events now appear to take place at the protein level, and are measurable  
585 with quantitative histology (see above).

586

587 **Gene set enrichment revealed early involvement of inflammation in the  $\alpha$ -syn**  
588 **seeding/spreading process**

589 To investigate which molecular pathways underlie the  $\alpha$ -syn spreading process and its  
590 associated pathologies, in particular microgliosis, we generated an enrichment map, using  
591 Gene-Set Enrichment Analysis (GSEA, see Methods), with each gene set based on a  
592 Biological Process (BP, see Methods for details). To obtain a global view of the BPs  
593 alterations during the evolution of  $\alpha$ -syn spreading induced pathologies, we used manual  
594 curation to group gene sets into biologically meaningful gene clusters associated with high  
595 order pathological processes (Fig. 7).

596 Our first observation was that, in ipsilateral midbrains of PFF-injected mice compared to  
597 those of PBS-injected ones, 261 BPs were enriched at 13 dpi, but, surprisingly none at 90 dpi.  
598 In contrast, we observed that, at 90 dpi, all BPs in ipsilateral midbrains of PFF-injected mice  
599 *versus* those of PBS-injected ones (total of 1067 BPs), showed reduced gene activity. This  
600 observation indicates a significant shift from enhanced to greatly reduced transcriptional

601 activity in the time frame between 13 dpi and 90 dpi, and confirms the observations on DEGs  
602 depicted in Fig. 6.

603 We then observed that many gene clusters with enhanced transcriptional activity at 13 dpi in  
604 ipsi PFF were associated with inflammation/immune processes (Fig. 7, upper panels), while  
605 gene clusters associated with similar activities had reduced transcriptional activity at 90 dpi,  
606 in particular compared to ipsi PBS (Fig. 7, lower left panel). This indicated that, after an  
607 initially enhanced activity of genes regulating inflammation/immune responses, that activity  
608 was strongly reduced at a stage when pathology was detectable histologically.

609 Another interesting observation we made was that some gene clusters containing BPs  
610 associated with reduced gene activity at 90 dpi, were related to dopaminergic neuron activity  
611 (e.g. catecholamine/dopamine metabolic processes, locomotor behavior, regulation of  
612 synaptic transmission regulation of signaling pathways upon growth factor stimulus). The  
613 reduced gene activity in midbrain dopaminergic neurons was likely a reflection of their  
614 pathological demise.

615 Taken together, these observations point to an important role for inflammatory/immune  
616 processes, in the initiation and progression of neurodegeneration in the context of  $\alpha$ -syn  
617 spreading.

618

### 619 **Gene expression changes confirm early microglial reaction in response to $\alpha$ -syn** 620 **seeding/spreading**

621 To identify the immune cell type(s) active in the inflammatory response to  $\alpha$ -syn  
622 seeding/spreading, we looked at the 20 most highly changed DEGs and their cellular source  
623 for each time points after PFF injection (Fig. 8). We used a public database based on single  
624 cell expression profiling from mouse brain to assign a cell type to each DEG in our list (see  
625 Methods).

626 At 13 dpi, in both the ipsi PFF *versus* ipsi PBS as well as the ipsi PFF *versus* contra PFF  
627 comparison, we observed that the majority of genes with enhanced expression were  
628 microglial (ipsi PFF *versus* ipsi PBS: 9 out of 20, or 45%, ipsi PFF *versus* contra PFF: 8 out  
629 of 20, or 40%). This indicates a strong gene expression activity of these cells, well before  
630 morphological changes can be detected histologically.

631 In contrast, at 90 dpi, we observed that only 1 out of 20 (5%) of DEGs was microglial in both  
632 comparisons (ipsi PFF *versus* ipsi PBS, ipsi PFF *versus* contra PFF). The majority (50%) of  
633 DEGs in the ipsi PFF *versus* ipsi PBS comparison were neuronal.

634 The observation that the majority of DEGs at 13 dpi were microglial, confirmed an early and  
635 strong response of these cells, at least on the molecular level.

636

637 **Unusual microglial molecular signature, induced by intrastriatal injection of  $\alpha$ -syn**  
638 **PFFs, precedes neurodegeneration**

639 To better understand the microglial molecular processes accompanying the  $\alpha$ -syn spreading  
640 process, we looked at expression of a series of genes coding for factors associated with  
641 typical pro-inflammatory (M1) or anti-inflammatory (M2) profile [76], with the same  
642 comparison pairs as before: ventral midbrains ipsi PFF *versus* ipsi PBS, and ventral  
643 midbrains ipsi PFF *versus* contra PFF (Table 1). In our model, we observed no clear-cut pro-  
644 inflammatory M1 nor anti-inflammatory M2-profile. Interestingly, we also observed no  
645 evidence, at 13 dpi or 90 dpi, for gene expression changes in classical M1 markers such as  
646 *Il1b*, *Tnfa*, or *Nos2*. M1 markers whose gene expression was enhanced were *Cybb*, *Ptgs2*, and  
647 *Cxcl10*. NADPH oxidase 2 (Nox2), coded by *Cybb*, generates free oxygen radicals, which  
648 can harm neurons [77]. Cyclooxygenase 2 (Cox2), coded by *Ptgs2*, generates arachidonic  
649 acid metabolites, some of which have been reported to be neurotoxic [78] or form neurotoxic

650 dopamine-quinone adducts [79]. Thus, this may be mediators of the neurodegeneration at 90  
651 dpi observed in ipsi PFF midbrains. The only M2 marker that showed enhanced gene  
652 expression was *Mrc1*, coding for the mannose receptor. Other microglial activation markers  
653 that have not been associated specifically with an M1 or M2 profile though, such as *Cd68*,  
654 *Tyrobd*, *Trem2*, *Tlr2*, *P2ry6*, and *Aif1*, showed increased expression at 13 dpi and/or 90 dpi.  
655 *Mrc1*, *Cd68*, *P2ry6*, *Aif1* gene products are all involved in phagocytic processes and/or signal  
656 transduction [80-82]. We had observed CD68 upregulation by immunostaining in the striatal  
657 projection area of dopaminergic neurons (Fig. 3). The *Tlr2* gene product is a receptor for  $\alpha$ -  
658 syn, an interaction that elicits the production of microglial neurotoxins [83], and anti-TLR2  
659 antibody administration has been reported to have therapeutic efficacy in mouse models of  $\alpha$ -  
660 syn toxicity [84]. *Tyrobp* and the gene for its receptor, *Trem2*, whose product is involved,  
661 among other processes in the regulation of microglial phagocytosis [85], were also  
662 upregulated.

663 Finally, to see if there was an astroglial and peripheral immune cell involvement in our  
664 model, we listed gene expression data for typical markers of these cells from our gene  
665 expression dataset (Supplemental table 3). Enhanced expression of a series of astroglial genes  
666 in ipsi PFF midbrain indicates a reaction of these cells. Enhanced expression of *Ptprc*, which  
667 codes for CD45, a marker that can be both expressed by microglia and invading  
668 macrophages, and of *Cd4*, which codes for the helper T cell antigen CD4, in the same region,  
669 indicates possible infiltration of peripheral immune cells that could contribute to neuronal  
670 injury [86-88]. Overall, we conclude that this unique molecular signature in the ipsilateral  
671 ventral midbrain at 13 dpi underlies the initial molecular events that lead to the  
672 neurodegeneration we observed at 90 dpi. Since neurodegeneration in the contralateral SN  
673 has been reported at later time points after PFF injection previously [20], in one study even in

674 the absence of  $\alpha$ -syn inclusions [89], it is reasonable to assume that, at a point past 13dpi, the  
675 same molecular signature occurs there.

676 Our data indicate that inflammatory events, in particular those associated with microglia, and  
677 not inclusion formation, are initiators of neurodegeneration in the context of  $\alpha$ -syn spreading  
678 in PD.

679

## 680 **Discussion**

681 In this study, we have used a seeding/spreading model of  $\alpha$ -syn, based on striatal injection of  
682 PFFs in the mouse brain, to investigate key questions on how two major pathological features  
683 of PD,  $\alpha$ -syn inclusion formation and neuroinflammation, contribute to neurodegeneration.

684 We provide evidence that: 1.  $\alpha$ -syn inclusion formation does not correlate with  
685 neurodegeneration: in areas with inclusions, the inclusion load did not correlate with the  
686 extent of neurodegeneration, and, in at least one area (hippocampus), neurodegeneration was  
687 detected in the absence of inclusions; 2. an exceptionally strong microglial response was seen  
688 across different brain regions, but this response did also not correlate with neurodegeneration;  
689 3. the most likely driver of the microglial response were diffusible  $\alpha$ -syn oligomers; 4. gene  
690 expression changes indicative of early neuroinflammatory events in the ventral midbrain, in  
691 particular in microglia, appeared before nigro-striatal degeneration, and some of these factors  
692 could be the driver for downstream neurodegeneration. Our study provides novel insights into  
693 underlying pathological processes of  $\alpha$ -syn spreading mediated PD-like neuronal injury.

694 We undertook this study because it is unclear how different pathological processes relate to  
695 each other in PD. In particular, it is intensely debated whether the  $\alpha$ -syn spreading and  
696 inclusion formation are the main driving forces in disease initiation and progression, or  
697 whether other processes do this or at least participate in them [90-92]. While the nature of the  
698 initial trigger of  $\alpha$ -syn's misfolding and seeding is still unknown, the hypothesis that its

699 spreading and seeding in a “prion-like” fashion along interconnected neuronal pathways,  
700 ultimately leading to inclusions, is a major driver of the PD pathological process has gained  
701 momentum [8, 93]. Observations on PD patients have provided indirect evidence for that  
702 view. For instance, the Braak hypothesis [10] posits that  $\alpha$ -syn pathology starts in lower  
703 motor nuclei of the brainstem (such as the Dorsal Motor Nucleus of the Vagus) or even in the  
704 PNS, then gradually moves upwards and, in doing so, causes various PD symptoms, from  
705 early non-motor to later motor and cognitive and psychiatric ones, to appear. Other routes of  
706 propagation, such as starting and spreading out from the olfactory bulb, have also been  
707 suggested [8]. Such a gradual progression of disease could elegantly be explained by  $\alpha$ -syn  
708 spreading like a prion. It was also observed that fetal grafts of dopaminergic neurons into the  
709 striatum of PD patients develop  $\alpha$ -syn inclusions after a few decades, which they could have  
710 acquired as consequence of  $\alpha$ -syn spreading from the surrounding disease tissue [12]. More  
711 direct evidence for the importance of  $\alpha$ -syn spreading in inducing PD-like disease comes  
712 from experimental models. In rodent or primate models, direct injection, in different brain  
713 regions, of PD brain tissue, isolated Lewy bodies, or PFF made out of recombinant  $\alpha$ -syn, or  
714 viral vector driven local overexpression of  $\alpha$ -syn, induces a variety of PD-related pathologies,  
715 including  $\alpha$ -syn spreading along connected neurons and inclusion formation [19]. Peripheral  
716 PFF injections, such as intramuscular or intestinal, have been reported to also lead to PD-like  
717 pathologies in the brain of mice [94-96]. These studies have cemented, experimentally, the  
718 process of “prion-like” propagation and inclusion formation of  $\alpha$ -syn.

719 The mechanism of this process has been investigated in *in vitro* systems. Cultured neurons  
720 secrete as well as take up circulating  $\alpha$ -syn, and various underlying mechanisms have been  
721 proposed, such as unusual forms of endo- and exocytosis, or nano-tubes [97]. Ingested,  
722 presumably misfolded  $\alpha$ -syn, corrupts its endogenous counterpart and leads it to form  
723 pathological inclusions [58]. During the process, different neuronal functions, such as axonal

724 transport or mitochondrial respiration, get impaired, neurons malfunction and may ultimately  
725 die [98, 99]. Glial cells have also been reported to take up  $\alpha$ -syn, and, in some cases, this can  
726 lead to pathological inclusions as well as in the case for oligodendrocytes in Multiple System  
727 Atrophy [100]. The toxic potential of inclusions has also been investigated *in vivo*. In a  
728 mouse model of  $\alpha$ -syn spreading, where inclusion formation was followed *in vivo* by multi-  
729 photon laser microscopy, the formation of intraneuronal inclusion was reported to coincide  
730 with neuronal dysfunction [33]. Another study has shown a weak correlation between loss of  
731 TH neurons in the SN and a global score of inclusion load after striatal PFF injection in both  
732 mice and rats, but a strong correlation between the two measures after direct injection of  
733 PFFs into the SN of rats [34]. Thus, it is tempting to conclude that  $\alpha$ -syn inclusions are at the  
734 very least one major driver of PD pathologies. But a closer look at other evidence reveals  
735 several unresolved questions in this otherwise elegant picture. In post-mortem brain tissues of  
736 early or late PD, the correlation between  $\alpha$ -syn inclusion (Lewy body) load and nigral  
737 degeneration is not always clear [25, 26]. Across different studies looking at various brain  
738 structures affected in PD,  $\alpha$ -syn inclusions have been reported in areas with high, moderate,  
739 or no neuronal loss [26]. Some PD patients, including some familial forms, have PD  
740 symptoms and loss of nigral neurons without detectable  $\alpha$ -syn inclusions [27]. Some neurons,  
741 such as GABAergic neurons, while appearing in the path of  $\alpha$ -syn spreading, never develop  
742 inclusions [27]. Interestingly, one study, comparing Incipient Lewy Body Disease (ILBD) to  
743 PD autopsy material, reported that neuronal loss precedes  $\alpha$ -syn inclusion formation in the  
744 SN [101]. In a rodent model where spreading is driven by viral overexpression of  $\alpha$ -syn in  
745 the Dorsal Motor Nucleus of the Vagus, while intact neuronal architecture was essential for  
746 the spreading process to happen, neurodegeneration and inclusion formation were also found  
747 to be independent processes [61].

748 Non-fibrillar forms of misfolded  $\alpha$ -syn, notably oligomers, diffusing for long distances within  
749 the brain, have been suggested to drive neuronal dysfunction and degeneration [30, 90]. In  
750 our study, we indeed found evidence for neurodegeneration that was independent of the  
751 presence of inclusions, and, in the hippocampus, even appeared in the complete absence of  
752 those, but in the presence of oligomers. Published evidence suggests that the hippocampus  
753 remains devoid of  $\alpha$ -syn inclusions even 180 days after PFF injection into the striatum [20].  
754 Our data therefore does not support the notion of a direct relationship between the formation  
755 of  $\alpha$ -syn inclusions and neurodegeneration, but rather indicate that the  $\alpha$ -syn spreading  
756 process may lead to the formation of pathological oligomers that may be the driver of PD-like  
757 neurodegeneration.

758 Pathologically misfolded  $\alpha$ -syn can drive neuronal injury in PD by different means, and those  
759 include mitochondrial dysfunction, oxidative stress, endoplasmic reticulum stress and  
760 lysosomal dysfunction, disequilibrium in cytosolic  $\text{Ca}^{2+}$ , neurotoxic oxidized dopamine,  
761 disruption of axonal transport, and neuroinflammation [99]. The relative contribution of these  
762 different processes to neuronal demise is unclear. Neuroinflammation though has received  
763 particular attention because of its widespread involvement in various neurological diseases  
764 and the potential for therapeutic modulation [75, 102, 103]. The major cellular mediators of  
765 this process are microglia. Microglia are a particular kind of myeloid cells that originate from  
766 the yolk sack and populate the nervous system during early stages of development, where  
767 they act as the innate, resident immune cells [67, 82]. During development and under normal  
768 conditions, they modulate nervous system homeostasis, prune synapses and regulate their  
769 formation. Under pathological conditions, they act as the primary line of defense against  
770 infectious organisms, and clear endogenous tissue debris after injury [37, 67, 82]. They  
771 undergo a substantial morphological and functional transition to activated, or reactive,  
772 microglia, which makes them functionally equivalent to macrophages [67]. Evidence



773 suggests though that, in many neurological conditions, they are not only reacting to disease,  
774 but play an active part in tissue injury exacerbation and propagation [82]. This pathological  
775 process is, in particular in PD, incompletely understood. While microglial activation can be  
776 induced by neuronal injury and/or misfolded and aggregated protein, notably  $\alpha$ -syn oligomers  
777 or fibrils [104], it is still unclear how and when microglial activation damages healthy tissue  
778 and exacerbates the neurological disease process. In PD, a strong microgliosis is observed  
779 *post mortem* in the SN [70, 105]. Longitudinal imaging studies with PET ligands  
780 demonstrated an early microglial activation in various regions beyond the SN, such as cortex,  
781 hippocampus, basal ganglia, and pons, but no correlation with other pathological measures,  
782 including clinical scores, of PD emerged [106, 107]. Interestingly, in striatal fetal grafts  
783 implanted in PD patients [12], microglia activation was observed years before the appearance  
784 of  $\alpha$ -syn inclusions [108]. In different toxin-induced PD rodent models, microgliosis was  
785 reported to precede, coincide, or follow the appearance of neuronal demise [70], while in a  
786 transgenic human  $\alpha$ -syn model [109] and in rats injected with PFFs into the striatum [110],  
787 microgliosis, measured histologically, was shown to precede neurodegeneration.  
788 These studies are based on the observation mainly, if not exclusively, of morphological  
789 changes of microglial response using immunostaining techniques for generic cell markers.  
790 While informative, the detection of morphological changes indicating microglial activation  
791 does not yield enough information on the actual physiological or molecular profile of these  
792 cells. The common distinction to characterize two functional states of activated microglia is  
793 the M1/M2 terminology, with M1 representing a pro-, whereas the M2 representing an anti-  
794 inflammatory activation status [76]. This distinction however is often inadequate as microglia  
795 commonly have a spectrum of activation states that may change over the course of the  
796 disease [111]. Recent gene expression profiling approaches have revealed a bewildering  
797 complexity in microglial heterogeneity [36, 112]. Evidence suggests a “core” gene expression

798 profile response that is associated with every neurodegeneration condition, while expression  
799 changes of a more restricted set of genes may be specific for each condition, leading to the  
800 concept of disease-specific microglial signatures [112]. Our study provides new insights into  
801 the molecular underpinnings of neuroinflammation preceding neuronal injury in a PD-like  
802 context of  $\alpha$ -syn spreading, and points to an active role of microglia in inducing  
803 neurodegeneration. First, we show, at the level of gene expression, that neuroinflammation-  
804 linked processes are activated, and that many microglial genes had increased expression  
805 levels at an early (13 dpi), which then were down-regulated at a later (90 dpi) time point after  
806 PFF injection. Microglia genes that code for factors causing neurodegeneration showed  
807 increased expression 13 dpi only in the ipsilateral midbrain, where TH loss was observed  
808 later, at 90 dpi. Among these were *Cybb*, which codes for NAPDH oxidase 2, an enzyme that  
809 catalyses the production of tissue harming free radicals [77], and *Ptgs2*, which codes for  
810 cyclooxygenase 2 (Cox2), an enzyme that forms prostanoids from arachidonic acid, some of  
811 which are neurotoxic [78, 113]. Interestingly, *Tlr2*, *Trem2*, and *Tyrobp* RNAs showed  
812 increased levels in our model at 13 dpi. Many genes linked to microglial activation are  
813 regulated by *Tyrobp*, a tyrosine kinase binding protein acting that binds to *Trem2*. The  
814 *Tyrobp/Trem2* pair triggers pathways that are involved in the inhibition of TLR-mediated  
815 inflammation, and in modulating phagocytosis [85]. *Tlr2*-deficient mice are protected against  
816 neurodegeneration induced by transgenic  $\alpha$ -syn overexpression [114]. In prodromal PD,  
817 TLR2 immunoreactivity on microglia was reported to be enhanced, whereas in late stage PD,  
818 it wasn't [115], indicating that, just like in our model, the microglial response happens in  
819 early phases of the disease and changes over time. Alpha-syn, in particular in its oligomeric  
820 form, activates microglia *in vitro* through Toll-like receptors [73, 104], and targeting TLR2  
821 by immunotherapy was shown to be beneficial in  $\alpha$ -syn pathology models [84].

822 The absence of increased gene expression of common pro-inflammatory mediators such as  
823 *Iilb* and *Tnfa* in our  $\alpha$ -syn spreading model is puzzling, since these are factors associated  
824 with most, if not all, inflammatory conditions. Of note though is that we also did not observe  
825 enhanced expression of these factors when primary microglia were exposed to our  $\alpha$ -syn  
826 PFFs, while they responded strongly to bacterial lipopolysaccharide (not shown). It is  
827 possible that the increased expression for these genes was missed and occurs at a time point  
828 after PFF injection that we haven't looked at, or that they are indeed not expressed in this  
829 model. Overall, the gene expression signature of microglia we detected was neither typical  
830 pro-inflammatory M1- nor anti-inflammatory M2-like, and our findings give further credence  
831 to the notion that microglia evolve on a spectrum of functional states as the disease  
832 progresses.

833

834 Taken together, our data indicate that, at least in the initial period of PD-like disease  
835 progression that is associated with  $\alpha$ -syn spreading, non-deposited pathological forms of  $\alpha$ -  
836 syn, such as oligomers, drive neurodegeneration in different brain regions *via* their action on  
837 microglia. Triggered microglia respond early, before neurodegeneration is apparent, by  
838 producing neurotoxic compounds, and through what appears to be a series of different  
839 activation states as the disease progresses. Our findings contribute toward first answers to key  
840 unresolved questions around neuroinflammation in PD [102], and have important  
841 implications for the design of therapeutic interventions during the early stages of the disease.

842

843

#### 844 ***Abbreviations***

845 6-OHDA:6-Hydroxydopamine; 13 dpi: 13 days post injection; 90 dpi: 90 days post injection;

846 A $\beta$ : amyloid beta peptide; AD: Alzheimer's disease;  $\alpha$ -syn: alpha-synuclein; BP: biological

847 process; CD68: cluster of differentiation 68; Contra: contralateral; COX2: Cyclooxygenase 2;  
848 CNS: central nervous system; DA: dopamine; DAT: dopamine transporter; DEG:  
849 differentially expressed gene; ES: enrichment score; FDR: false discovery rate; GO: gene  
850 ontology; GSEA: gene set enrichment analysis; Iba1: ionized calcium binding adaptor  
851 molecule; Ipsi: ipsilateral; PBS: phosphate-buffered saline; PET assay: paraffin-embedded  
852 tissue assay; PFF: Pre-formed fibril; Pfp: percent false positives; PLA: proximity ligation  
853 assay  
854 p-SER129- $\alpha$ -syn: alpha-synuclein phosphorylated at serine position 129; SN: Substantia  
855 Nigra; TDP43: TAR DNA-binding protein 43; TH: tyrosine-hydroxylase; TLR2: Toll-like  
856 receptor 2; WB: Western blot.

857

## 858 **Additional information**

### 859 *Ethics approval*

860 Animal studies performed at the Luxembourg Centre for Systems Biomedicine were  
861 approved by the institutional Animal Experimentation Ethics Committee of the University of  
862 Luxembourg, and the responsible Luxembourg government authorities (Ministry of Health,  
863 Ministry of Agriculture). Alternatively, experiments done at the SynAging site were  
864 approved by ethics committee “Comité d’Ethique Lorrain en Matière d’Expérimentation  
865 Animale”, and by the governmental agency the “Direction Départementale de la Protection  
866 des Populations de Meurthe et Moselle- Domaine Expérimentation Animale”.

867

### 868 *Consent for publication*

869 All authors have approved of the contents of this manuscript and provided consent for  
870 publication.

871

872 *Availability of materials*

873 Alpha-synuclein PFFs, the 11A5 monoclonal anti  $\alpha$ -synuclein antibody, and the  $\alpha$ -syn  
874 oligomers can be obtained, under MTAs, from Biogen, Prothena Biosciences, and ETAP-lab,  
875 respectively.

876

877 *Funding*

878 Wiebke Wemheuer was a recipient of a postdoctoral fellowship from the Luxembourg  
879 National Research Fond, Luxembourg (FNR AFR 5712281). Michel Mittelbronn thanks the  
880 Luxembourg National Research Fond (FNR) for support (FNR PEARL P16/BM/11192868  
881 grant).

882

883 *Authors contributions*

884 P.G., W.W., D.C., and M.B, designed the study. P.G., W.W., O.H., A.Ma., S.B., E.K., T.H.,  
885 A.W., C.S., A. Mi., T.P., A.A., N.F. did the experiments (stereotactic surgery, tissue  
886 processing, stainings, imaging and RNA extraction). T.K., N.N. generated the microarray  
887 data. K.J.S., E.G. analyzed the microarray data. P.G., W.W., O.H., K.J.S., R.B., W.S.-S.,  
888 K.B., M.M., M.B analyzed and interpreted the data. M.B. wrote the paper. All authors read  
889 and approved the final manuscript.

890

891 *Acknowledgements*

892 We thank Laurent Vallar (Luxembourg Institute of Health) for help with gene expression  
893 arrays, Christian Jaeger (Luxembourg Centre for Systems Biomedicine) for dopamine  
894 measurements, Eliezer Masliah (University of California, San Diego) for advice, Thierry  
895 Pillot and Violette Koziel (SynAging, France) for synuclein oligomers and for advice, and  
896 Yuting Liu (Biogen) for purifying recombinant murine  $\alpha$ -syn. We also thank Prothena  
897 Biosciences (South San Francisco, CA) for providing the 11A5 antibody.

898

899

900 **References**

- 901 1. Chiti F, Dobson CM: **Protein Misfolding, Amyloid Formation, and Human**  
902 **Disease: A Summary of Progress Over the Last Decade.** *Annu Rev Biochem* 2017,  
903 **86:27-68.**
- 904 2. Selkoe DJ: **Folding proteins in fatal ways.** *Nature* 2003, **426:900-904.**
- 905 3. Scheckel C, Aguzzi A: **Prions, prionoids and protein misfolding disorders.** *Nat*  
906 *Rev Genet* 2018, **19:405-418.**
- 907 4. Goedert M: **NEURODEGENERATION. Alzheimer's and Parkinson's diseases:**  
908 **The prion concept in relation to assembled Abeta, tau, and alpha-synuclein.**  
909 *Science* 2015, **349:1255-555.**
- 910 5. Ross CA, Poirier MA: **Protein aggregation and neurodegenerative disease.** *Nat*  
911 *Med* 2004, **10 Suppl:S10-17.**
- 912 6. Walker LC, Jucker M: **Neurodegenerative diseases: expanding the prion concept.**  
913 *Annu Rev Neurosci* 2015, **38:87-103.**
- 914 7. Jucker M, Walker LC: **Propagation and spread of pathogenic protein assemblies**  
915 **in neurodegenerative diseases.** *Nat Neurosci* 2018, **21:1341-1349.**
- 916 8. Meziaris C, Rey N, Brundin P, Raj A: **Neural connectivity predicts spreading of**  
917 **alpha-synuclein pathology in fibril-injected mouse models: Involvement of**  
918 **retrograde and anterograde axonal propagation.** *Neurobiol Dis* 2020, **134:104623.**
- 919 9. Braak H, Braak E: **Staging of Alzheimer's disease-related neurofibrillary changes.**  
920 *Neurobiol Aging* 1995, **16:271-278**; discussion 278-284.
- 921 10. Braak H, Del Tredici K, Rub U, de Vos RA, Jansen Steur EN, Braak E: **Staging of**  
922 **brain pathology related to sporadic Parkinson's disease.** *Neurobiol Aging* 2003,  
923 **24:197-211.**
- 924 11. Brundin P, Ma J, Kordower JH: **How strong is the evidence that Parkinson's**  
925 **disease is a prion disorder?** *Curr Opin Neurol* 2016, **29:459-466.**
- 926 12. Chu Y, Kordower JH: **Lewy body pathology in fetal grafts.** *Ann N Y Acad Sci* 2010,  
927 **1184:55-67.**
- 928 13. Bendor JT, Logan TP, Edwards RH: **The function of alpha-synuclein.** *Neuron* 2013,  
929 **79:1044-1066.**
- 930 14. Burre J, Sharma M, Sudhof TC: **Cell Biology and Pathophysiology of alpha-**  
931 **Synuclein.** *Cold Spring Harb Perspect Med* 2018, **8.**
- 932 15. Spillantini MG, Crowther RA, Jakes R, Hasegawa M, Goedert M: **alpha-Synuclein**  
933 **in filamentous inclusions of Lewy bodies from Parkinson's disease and dementia**  
934 **with lewy bodies.** *Proc Natl Acad Sci U S A* 1998, **95:6469-6473.**
- 935 16. Singleton A, Hardy J: **Progress in the genetic analysis of Parkinson's disease.** *Hum*  
936 *Mol Genet* 2019, **28:R215-R218.**
- 937 17. Lin MK, Farrer MJ: **Genetics and genomics of Parkinson's disease.** *Genome Med*  
938 2014, **6:48.**
- 939 18. Chu Y, Muller S, Tavares A, Barret O, Alagille D, Seibyl J, Tamagnan G, Marek K,  
940 Luk KC, Trojanowski JQ, et al: **Intrastriatal alpha-synuclein fibrils in monkeys:**  
941 **spreading, imaging and neuropathological changes.** *Brain* 2019, **142:3565-3579.**
- 942 19. Rey NL, George S, Brundin P: **Review: Spreading the word: precise animal**  
943 **models and validated methods are vital when evaluating prion-like behaviour of**  
944 **alpha-synuclein.** *Neuropathol Appl Neurobiol* 2016, **42:51-76.**
- 945 20. Luk KC, Kehm V, Carroll J, Zhang B, O'Brien P, Trojanowski JQ, Lee VM:  
946 **Pathological alpha-synuclein transmission initiates Parkinson-like**  
947 **neurodegeneration in nontransgenic mice.** *Science* 2012, **338:949-953.**

- 948 21. Luna E, Luk KC: **Bent out of shape: alpha-Synuclein misfolding and the**  
949 **convergence of pathogenic pathways in Parkinson's disease.** *FEBS Lett* 2015,  
950 **589:3749-3759.**
- 951 22. Ulusoy A, Rusconi R, Perez-Revuelta BI, Musgrove RE, Helwig M, Winzen-Reichert  
952 B, Di Monte DA: **Caudo-rostral brain spreading of alpha-synuclein through**  
953 **vagal connections.** *EMBO Mol Med* 2013, **5:1119-1127.**
- 954 23. Dijkstra AA, Voorn P, Berendse HW, Groenewegen HJ, Netherlands Brain B,  
955 Rozemuller AJ, van de Berg WD: **Stage-dependent nigral neuronal loss in**  
956 **incidental Lewy body and Parkinson's disease.** *Mov Disord* 2014, **29:1244-1251.**
- 957 24. Espay AJ, Marras C: **Clinical Parkinson disease subtyping does not predict**  
958 **pathology.** *Nat Rev Neurol* 2019, **15:189-190.**
- 959 25. Jellinger KA: **A critical evaluation of current staging of alpha-synuclein**  
960 **pathology in Lewy body disorders.** *Biochim Biophys Acta* 2009, **1792:730-740.**
- 961 26. Jellinger KA: **Formation and development of Lewy pathology: a critical update.** *J*  
962 *Neurol* 2009, **256 Suppl 3:270-279.**
- 963 27. Surmeier DJ, Obeso JA, Halliday GM: **Selective neuronal vulnerability in**  
964 **Parkinson disease.** *Nat Rev Neurosci* 2017, **18:101-113.**
- 965 28. Poewe W, Seppi K, Tanner CM, Halliday GM, Brundin P, Volkman J, Schrag AE,  
966 Lang AE: **Parkinson disease.** *Nat Rev Dis Primers* 2017, **3:17013.**
- 967 29. Walsh DM, Selkoe DJ: **Oligomers on the brain: the emerging role of soluble**  
968 **protein aggregates in neurodegeneration.** *Protein Pept Lett* 2004, **11:213-228.**
- 969 30. Bengoa-Vergniory N, Roberts RF, Wade-Martins R, Alegre-Abarrategui J: **Alpha-**  
970 **synuclein oligomers: a new hope.** *Acta Neuropathol* 2017, **134:819-838.**
- 971 31. Mucke L, Selkoe DJ: **Neurotoxicity of amyloid beta-protein: synaptic and**  
972 **network dysfunction.** *Cold Spring Harb Perspect Med* 2012, **2:a006338.**
- 973 32. Helwig M, Klinkenberg M, Rusconi R, Musgrove RE, Majbour NK, El-Agnaf OM,  
974 Ulusoy A, Di Monte DA: **Brain propagation of transduced alpha-synuclein**  
975 **involves non-fibrillar protein species and is enhanced in alpha-synuclein null**  
976 **mice.** *Brain* 2016, **139:856-870.**
- 977 33. Osterberg VR, Spinelli KJ, Weston LJ, Luk KC, Woltjer RL, Unni VK: **Progressive**  
978 **aggregation of alpha-synuclein and selective degeneration of lewy inclusion-**  
979 **bearing neurons in a mouse model of parkinsonism.** *Cell Rep* 2015, **10:1252-1260.**
- 980 34. Abdelmotilib H, Maltbie T, Delic V, Liu Z, Hu X, Fraser KB, Moehle MS, Stoyka L,  
981 Anabtawi N, Krendelchtchikova V, et al: **alpha-Synuclein fibril-induced inclusion**  
982 **spread in rats and mice correlates with dopaminergic Neurodegeneration.**  
983 *Neurobiol Dis* 2017, **105:84-98.**
- 984 35. Hammond TR, Marsh SE, Stevens B: **Immune Signaling in Neurodegeneration.**  
985 *Immunity* 2019, **50:955-974.**
- 986 36. Crotti A, Ransohoff RM: **Microglial Physiology and Pathophysiology: Insights**  
987 **from Genome-wide Transcriptional Profiling.** *Immunity* 2016, **44:505-515.**
- 988 37. Wolf SA, Boddeke HW, Kettenmann H: **Microglia in Physiology and Disease.** *Annu*  
989 *Rev Physiol* 2017, **79:619-643.**
- 990 38. Weihofen A, Liu Y, Arndt JW, Huy C, Quan C, Smith BA, Baeriswyl JL, Cavegn N,  
991 Senn L, Su L, et al: **Development of an aggregate-selective, human-derived alpha-**  
992 **synuclein antibody BIIB054 that ameliorates disease phenotypes in Parkinson's**  
993 **disease models.** *Neurobiol Dis* 2019, **124:276-288.**
- 994 39. Malaplate-Armand C, Florent-Bechard S, Youssef I, Koziel V, Sponne I, Kriem B,  
995 Leininger-Muller B, Olivier JL, Oster T, Pillot T: **Soluble oligomers of amyloid-beta**  
996 **peptide induce neuronal apoptosis by activating a cPLA2-dependent**  
997 **sphingomyelinase-ceramide pathway.** *Neurobiol Dis* 2006, **23:178-189.**



- 998 40. Almandoz-Gil L, Ingelsson M, Bergstrom J: **Generation and Characterization of**  
999 **Stable alpha-Synuclein Oligomers.** *Methods Mol Biol* 2018, **1779**:61-71.
- 1000 41. Buttini M, Masliah E, Barbour R, Grajeda H, Motter R, Johnson-Wood K, Khan K,  
1001 Seubert P, Freedman S, Schenk D, Games D: **Beta-amyloid immunotherapy**  
1002 **prevents synaptic degeneration in a mouse model of Alzheimer's disease.** *J*  
1003 *Neurosci* 2005, **25**:9096-9101.
- 1004 42. Buttini M, Orth M, Bellosta S, Akeefe H, Pitas RE, Wyss-Coray T, Mucke L, Mahley  
1005 RW: **Expression of human apolipoprotein E3 or E4 in the brains of Apoe<sup>-/-</sup> mice:**  
1006 **isoform-specific effects on neurodegeneration.** *J Neurosci* 1999, **19**:4867-4880.
- 1007 43. Jaeger C, Glaab E, Michelucci A, Binz TM, Koeglsberger S, Garcia P, Trezzi JP,  
1008 Ghelfi J, Balling R, Buttini M: **The mouse brain metabolome: region-specific**  
1009 **signatures and response to excitotoxic neuronal injury.** *Am J Pathol* 2015,  
1010 **185**:1699-1712.
- 1011 44. Cabeza-Arvelaiz Y, Fleming SM, Richter F, Masliah E, Chesselet MF, Schiestl RH:  
1012 **Analysis of striatal transcriptome in mice overexpressing human wild-type**  
1013 **alpha-synuclein supports synaptic dysfunction and suggests mechanisms of**  
1014 **neuroprotection for striatal neurons.** *Mol Neurodegener* 2011, **6**:83.
- 1015 45. Miller RM, Kiser GL, Kaysser-Kranich T, Casaceli C, Colla E, Lee MK, Palaniappan  
1016 C, Federoff HJ: **Wild-type and mutant alpha-synuclein induce a multi-component**  
1017 **gene expression profile consistent with shared pathophysiology in different**  
1018 **transgenic mouse models of PD.** *Exp Neurol* 2007, **204**:421-432.
- 1019 46. Paxinos G, Franklin, K. : **The mouse brain atlas in stereotactic coordinates.**  
1020 *Elsevier Academic Press* 2008, **3rd edition.**
- 1021 47. Ashrafi A, Garcia P, Kollmus H, Schughart K, Del Sol A, Buttini M, Glaab E:  
1022 **Absence of regulator of G-protein signaling 4 does not protect against dopamine**  
1023 **neuron dysfunction and injury in the mouse 6-hydroxydopamine lesion model of**  
1024 **Parkinson's disease.** *Neurobiol Aging* 2017, **58**:30-33.
- 1025 48. Jager C, Hiller K, Buttini M: **Metabolic Profiling and Quantification of**  
1026 **Neurotransmitters in Mouse Brain by Gas Chromatography-Mass Spectrometry.**  
1027 *Curr Protoc Mouse Biol* 2016, **6**:333-342.
- 1028 49. Kramer ML, Schulz-Schaeffer WJ: **Presynaptic alpha-synuclein aggregates, not**  
1029 **Lewy bodies, cause neurodegeneration in dementia with Lewy bodies.** *J Neurosci*  
1030 2007, **27**:1405-1410.
- 1031 50. Trifilieff P, Rives ML, Urizar E, Piskorowski RA, Vishwasrao HD, Castrillon J,  
1032 Schmauss C, Slattman M, Gullberg M, Javitch JA: **Detection of antigen interactions**  
1033 **ex vivo by proximity ligation assay: endogenous dopamine D2-adenosine A2A**  
1034 **receptor complexes in the striatum.** *Biotechniques* 2011, **51**:111-118.
- 1035 51. Bougnaud S, Golebiewska A, Oudin A, Keunen O, Harter PN, Mader L, Azuaje F,  
1036 Fritah S, Stieber D, Kaoma T, et al: **Molecular crosstalk between tumour and brain**  
1037 **parenchyma instructs histopathological features in glioblastoma.** *Oncotarget*  
1038 2016, **7**:31955-31971.
- 1039 52. Breitling R, Armengaud P, Amtmann A, Herzyk P: **Rank products: a simple, yet**  
1040 **powerful, new method to detect differentially regulated genes in replicated**  
1041 **microarray experiments.** *FEBS Lett* 2004, **573**:83-92.
- 1042 53. Del Carratore F, Jankevics A, Eisinga R, Heskes T, Hong F, Breitling R: **RankProd**  
1043 **2.0: a refactored bioconductor package for detecting differentially expressed**  
1044 **features in molecular profiling datasets.** *Bioinformatics* 2017, **33**:2774-2775.
- 1045 54. Hong F, Breitling R, McEntee CW, Wittner BS, Nemhauser JL, Chory J: **RankProd:**  
1046 **a bioconductor package for detecting differentially expressed genes in meta-**  
1047 **analysis.** *Bioinformatics* 2006, **22**:2825-2827.

- 1048 55. Subramanian A, Tamayo P, Mootha VK, Mukherjee S, Ebert BL, Gillette MA,  
1049 Paulovich A, Pomeroy SL, Golub TR, Lander ES, Mesirov JP: **Gene set enrichment**  
1050 **analysis: a knowledge-based approach for interpreting genome-wide expression**  
1051 **profiles.** *Proc Natl Acad Sci U S A* 2005, **102**:15545-15550.
- 1052 56. Benjamini YHY: **Controlling the False Discovery Rate: A Practical and Powerful**  
1053 **Approach to Multiple Testing.** *Journal of the Royal Statistical Society Sries B*  
1054 *(Methodological)* 1995, **57**:289-300.
- 1055 57. Shannon P, Markiel A, Ozier O, Baliga NS, Wang JT, Ramage D, Amin N,  
1056 Schwikowski B, Ideker T: **Cytoscape: a software environment for integrated**  
1057 **models of biomolecular interaction networks.** *Genome Res* 2003, **13**:2498-2504.
- 1058 58. Spillantini MG, Goedert M: **Neurodegeneration and the ordered assembly of**  
1059 **alpha-synuclein.** *Cell Tissue Res* 2018, **373**:137-148.
- 1060 59. Vaikath NN, Hmila I, Gupta V, Erskine D, Ingelsson M, El-Agnaf OMA: **Antibodies**  
1061 **against alpha-synuclein: tools and therapies.** *J Neurochem* 2019, **150**:612-625.
- 1062 60. Roberts RF, Wade-Martins R, Alegre-Abarrategui J: **Direct visualization of alpha-**  
1063 **synuclein oligomers reveals previously undetected pathology in Parkinson's**  
1064 **disease brain.** *Brain* 2015, **138**:1642-1657.
- 1065 61. Ulusoy A, Musgrove RE, Rusconi R, Klinkenberg M, Helwig M, Schneider A, Di  
1066 Monte DA: **Neuron-to-neuron alpha-synuclein propagation in vivo is**  
1067 **independent of neuronal injury.** *Acta Neuropathol Commun* 2015, **3**:13.
- 1068 62. Calhoun ME, Jucker M, Martin LJ, Thinakaran G, Price DL, Mouton PR:  
1069 **Comparative evaluation of synaptophysin-based methods for quantification of**  
1070 **synapses.** *J Neurocytol* 1996, **25**:821-828.
- 1071 63. Zhan SS, Beyreuther K, Schmitt HP: **Quantitative assessment of the synaptophysin**  
1072 **immuno-reactivity of the cortical neuropil in various neurodegenerative**  
1073 **disorders with dementia.** *Dementia* 1993, **4**:66-74.
- 1074 64. Bellucci A, Mercuri NB, Venneri A, Faustini G, Longhena F, Pizzi M, Missale C,  
1075 Spano P: **Review: Parkinson's disease: from synaptic loss to connectome**  
1076 **dysfunction.** *Neuropathol Appl Neurobiol* 2016, **42**:77-94.
- 1077 65. Aarsland D, Creese B, Politis M, Chaudhuri KR, Ffytche DH, Weintraub D, Ballard  
1078 C: **Cognitive decline in Parkinson disease.** *Nat Rev Neurol* 2017, **13**:217-231.
- 1079 66. Wu Q, Takano H, Riddle DM, Trojanowski JQ, Coulter DA, Lee VM: **alpha-**  
1080 **Synuclein (alphaSyn) Preformed Fibrils Induce Endogenous alphaSyn**  
1081 **Aggregation, Compromise Synaptic Activity and Enhance Synapse Loss in**  
1082 **Cultured Excitatory Hippocampal Neurons.** *J Neurosci* 2019, **39**:5080-5094.
- 1083 67. Michelucci A, Mittelbronn M, Gomez-Nicola D: **Microglia in Health and Disease:**  
1084 **A Unique Immune Cell Population.** *Front Immunol* 2018, **9**:1779.
- 1085 68. Biber K, Owens T, Boddeke E: **What is microglia neurotoxicity (Not)?** *Glia* 2014,  
1086 **62**:841-854.
- 1087 69. Doorn KJ, Lucassen PJ, Boddeke HW, Prins M, Berendse HW, Drukarch B, van Dam  
1088 AM: **Emerging roles of microglial activation and non-motor symptoms in**  
1089 **Parkinson's disease.** *Prog Neurobiol* 2012, **98**:222-238.
- 1090 70. Joers V, Tansey MG, Mulas G, Carta AR: **Microglial phenotypes in Parkinson's**  
1091 **disease and animal models of the disease.** *Prog Neurobiol* 2017, **155**:57-75.
- 1092 71. Tan EK, Chao YX, West A, Chan LL, Poewe W, Jankovic J: **Parkinson disease and**  
1093 **the immune system - associations, mechanisms and therapeutics.** *Nat Rev Neurol*  
1094 2020.
- 1095 72. Fu R, Shen Q, Xu P, Luo JJ, Tang Y: **Phagocytosis of microglia in the central**  
1096 **nervous system diseases.** *Mol Neurobiol* 2014, **49**:1422-1434.

- 1097 73. Kim C, Ho DH, Suk JE, You S, Michael S, Kang J, Joong Lee S, Masliah E, Hwang  
1098 D, Lee HJ, Lee SJ: **Neuron-released oligomeric alpha-synuclein is an endogenous**  
1099 **agonist of TLR2 for paracrine activation of microglia.** *Nat Commun* 2013, **4**:1562.
- 1100 74. Hughes CD, Choi ML, Ryten M, Hopkins L, Drews A, Botia JA, Iljina M, Rodrigues  
1101 M, Gagliano SA, Gandhi S, et al: **Picomolar concentrations of oligomeric alpha-**  
1102 **synuclein sensitizes TLR4 to play an initiating role in Parkinson's disease**  
1103 **pathogenesis.** *Acta Neuropathol* 2019, **137**:103-120.
- 1104 75. Tansey MG, Romero-Ramos M: **Immune system responses in Parkinson's disease:**  
1105 **Early and dynamic.** *Eur J Neurosci* 2019, **49**:364-383.
- 1106 76. Tang Y, Le W: **Differential Roles of M1 and M2 Microglia in Neurodegenerative**  
1107 **Diseases.** *Mol Neurobiol* 2016, **53**:1181-1194.
- 1108 77. Ma MW, Wang J, Zhang Q, Wang R, Dhandapani KM, Vadlamudi RK, Brann DW:  
1109 **NADPH oxidase in brain injury and neurodegenerative disorders.** *Mol*  
1110 *Neurodegener* 2017, **12**:7.
- 1111 78. Figueiredo-Pereira ME, Corwin C, Babich J: **Prostaglandin J2: a potential target**  
1112 **for halting inflammation-induced neurodegeneration.** *Ann N Y Acad Sci* 2016,  
1113 **1363**:125-137.
- 1114 79. Teismann P, Tieu K, Choi DK, Wu DC, Naini A, Hunot S, Vila M, Jackson-Lewis V,  
1115 Przedborski S: **Cyclooxygenase-2 is instrumental in Parkinson's disease**  
1116 **neurodegeneration.** *Proc Natl Acad Sci U S A* 2003, **100**:5473-5478.
- 1117 80. Janda E, Boi L, Carta AR: **Microglial Phagocytosis and Its Regulation: A**  
1118 **Therapeutic Target in Parkinson's Disease?** *Front Mol Neurosci* 2018, **11**:144.
- 1119 81. Bhattacharya A, Biber K: **The microglial ATP-gated ion channel P2X7 as a CNS**  
1120 **drug target.** *Glia* 2016, **64**:1772-1787.
- 1121 82. Ransohoff RM, El Khoury J: **Microglia in Health and Disease.** *Cold Spring Harb*  
1122 *Perspect Biol* 2015, **8**:a020560.
- 1123 83. Kim C, Lee HJ, Masliah E, Lee SJ: **Non-cell-autonomous Neurotoxicity of alpha-**  
1124 **synuclein Through Microglial Toll-like Receptor 2.** *Exp Neurobiol* 2016, **25**:113-  
1125 119.
- 1126 84. Kim C, Spencer B, Rockenstein E, Yamakado H, Mante M, Adame A, Fields JA,  
1127 Masliah D, Iba M, Lee HJ, et al: **Immunotherapy targeting toll-like receptor 2**  
1128 **alleviates neurodegeneration in models of synucleinopathy by modulating alpha-**  
1129 **synuclein transmission and neuroinflammation.** *Mol Neurodegener* 2018, **13**:43.
- 1130 85. Konishi H, Kiyama H: **Microglial TREM2/DAP12 Signaling: A Double-Edged**  
1131 **Sword in Neural Diseases.** *Front Cell Neurosci* 2018, **12**:206.
- 1132 86. Brochard V, Combadiere B, Prigent A, Laouar Y, Perrin A, Beray-Berthet V,  
1133 Bonduelle O, Alvarez-Fischer D, Callebert J, Launay JM, et al: **Infiltration of CD4+**  
1134 **lymphocytes into the brain contributes to neurodegeneration in a mouse model**  
1135 **of Parkinson disease.** *J Clin Invest* 2009, **119**:182-192.
- 1136 87. Harms AS, Delic V, Thome AD, Bryant N, Liu Z, Chandra S, Jurkuvenaite A, West  
1137 AB: **alpha-Synuclein fibrils recruit peripheral immune cells in the rat brain**  
1138 **prior to neurodegeneration.** *Acta Neuropathol Commun* 2017, **5**:85.
- 1139 88. Kannarkat GT, Boss JM, Tansey MG: **The role of innate and adaptive immunity in**  
1140 **Parkinson's disease.** *J Parkinsons Dis* 2013, **3**:493-514.
- 1141 89. Paumier KL, Luk KC, Manfredsson FP, Kanaan NM, Lipton JW, Collier TJ, Steece-  
1142 Collier K, Kemp CJ, Celano S, Schulz E, et al: **Intrastriatal injection of pre-formed**  
1143 **mouse alpha-synuclein fibrils into rats triggers alpha-synuclein pathology and**  
1144 **bilateral nigrostriatal degeneration.** *Neurobiol Dis* 2015, **82**:185-199.
- 1145 90. Walsh DM, Selkoe DJ: **A critical appraisal of the pathogenic protein spread**  
1146 **hypothesis of neurodegeneration.** *Nat Rev Neurosci* 2016, **17**:251-260.

- 1147 91. Brundin P, Melki R: **Prying into the Prion Hypothesis for Parkinson's Disease.** *J*  
1148 *Neurosci* 2017, **37**:9808-9818.
- 1149 92. Surmeier DJ, Obeso JA, Halliday GM: **Parkinson's Disease Is Not Simply a Prion**  
1150 **Disorder.** *J Neurosci* 2017, **37**:9799-9807.
- 1151 93. Goedert M, Jakes R, Spillantini MG: **The Synucleinopathies: Twenty Years On.** *J*  
1152 *Parkinsons Dis* 2017, **7**:S51-S69.
- 1153 94. Ayers JI, Brooks MM, Rutherford NJ, Howard JK, Sorrentino ZA, Riffe CJ, Giasson  
1154 BI: **Robust Central Nervous System Pathology in Transgenic Mice following**  
1155 **Peripheral Injection of alpha-Synuclein Fibrils.** *J Virol* 2017, **91**.
- 1156 95. Holmqvist S, Chutna O, Bousset L, Aldrin-Kirk P, Li W, Bjorklund T, Wang ZY,  
1157 Roybon L, Melki R, Li JY: **Direct evidence of Parkinson pathology spread from**  
1158 **the gastrointestinal tract to the brain in rats.** *Acta Neuropathol* 2014, **128**:805-820.
- 1159 96. Sacino AN, Brooks M, Thomas MA, McKinney AB, Lee S, Regenhardt RW,  
1160 McGarvey NH, Ayers JI, Notterpek L, Borchelt DR, et al: **Intramuscular injection**  
1161 **of alpha-synuclein induces CNS alpha-synuclein pathology and a rapid-onset**  
1162 **motor phenotype in transgenic mice.** *Proc Natl Acad Sci U S A* 2014, **111**:10732-  
1163 10737.
- 1164 97. Rodriguez L, Marano MM, Tandon A: **Import and Export of Misfolded alpha-**  
1165 **Synuclein.** *Front Neurosci* 2018, **12**:344.
- 1166 98. Lashuel HA, Overk CR, Oueslati A, Masliah E: **The many faces of alpha-synuclein:**  
1167 **from structure and toxicity to therapeutic target.** *Nat Rev Neurosci* 2013, **14**:38-  
1168 48.
- 1169 99. Rocha EM, De Miranda B, Sanders LH: **Alpha-synuclein: Pathology,**  
1170 **mitochondrial dysfunction and neuroinflammation in Parkinson's disease.**  
1171 *Neurobiol Dis* 2018, **109**:249-257.
- 1172 100. Filippini A, Gennarelli M, Russo I: **alpha-Synuclein and Glia in Parkinson's**  
1173 **Disease: A Beneficial or a Detrimental Duet for the Endo-Lysosomal System?**  
1174 *Cell Mol Neurobiol* 2019, **39**:161-168.
- 1175 101. Milber JM, Noorigian JV, Morley JF, Petrovitch H, White L, Ross GW, Duda JE:  
1176 **Lewy pathology is not the first sign of degeneration in vulnerable neurons in**  
1177 **Parkinson disease.** *Neurology* 2012, **79**:2307-2314.
- 1178 102. Hirsch EC, Standaert DG: **Ten Unsolved Questions About Neuroinflammation in**  
1179 **Parkinson's Disease.** *Mov Disord* 2020.
- 1180 103. Lema Tome CM, Tyson T, Rey NL, Grathwohl S, Britschgi M, Brundin P:  
1181 **Inflammation and alpha-synuclein's prion-like behavior in Parkinson's disease--**  
1182 **is there a link?** *Mol Neurobiol* 2013, **47**:561-574.
- 1183 104. Fellner L, Irschick R, Schanda K, Reindl M, Klimaschewski L, Poewe W, Wenning  
1184 GK, Stefanova N: **Toll-like receptor 4 is required for alpha-synuclein dependent**  
1185 **activation of microglia and astroglia.** *Glia* 2013, **61**:349-360.
- 1186 105. Croisier E, Moran LB, Dexter DT, Pearce RK, Graeber MB: **Microglial**  
1187 **inflammation in the parkinsonian substantia nigra: relationship to alpha-**  
1188 **synuclein deposition.** *J Neuroinflammation* 2005, **2**:14.
- 1189 106. Gerhard A, Pavese N, Hotton G, Turkheimer F, Es M, Hammers A, Eggert K, Oertel  
1190 W, Banati RB, Brooks DJ: **In vivo imaging of microglial activation with [11C](R)-**  
1191 **PK11195 PET in idiopathic Parkinson's disease.** *Neurobiol Dis* 2006, **21**:404-412.
- 1192 107. Terada T, Yokokura M, Yoshikawa E, Futatsubashi M, Kono S, Konishi T, Miyajima  
1193 H, Hashizume T, Ouchi Y: **Extrastriatal spreading of microglial activation in**  
1194 **Parkinson's disease: a positron emission tomography study.** *Ann Nucl Med* 2016,  
1195 **30**:579-587.

- 1196 108. Olanow CW, Savolainen M, Chu Y, Halliday GM, Kordower JH: **Temporal**  
1197 **evolution of microglia and alpha-synuclein accumulation following foetal**  
1198 **grafting in Parkinson's disease.** *Brain* 2019, **142**:1690-1700.
- 1199 109. Watson MB, Richter F, Lee SK, Gabby L, Wu J, Masliah E, Effros RB, Chesselet  
1200 MF: **Regionally-specific microglial activation in young mice over-expressing**  
1201 **human wildtype alpha-synuclein.** *Exp Neurol* 2012, **237**:318-334.
- 1202 110. Duffy MF, Collier TJ, Patterson JR, Kemp CJ, Luk KC, Tansey MG, Paumier KL,  
1203 Kanaan NM, Fischer DL, Polinski NK, et al: **Lewy body-like alpha-synuclein**  
1204 **inclusions trigger reactive microgliosis prior to nigral degeneration.** *J*  
1205 *Neuroinflammation* 2018, **15**:129.
- 1206 111. Ransohoff RM: **A polarizing question: do M1 and M2 microglia exist?** *Nat*  
1207 *Neurosci* 2016, **19**:987-991.
- 1208 112. Dubbelaar ML, Kracht L, Eggen BJL, Boddeke E: **The Kaleidoscope of Microglial**  
1209 **Phenotypes.** *Front Immunol* 2018, **9**:1753.
- 1210 113. Hsieh YC, Mounsey RB, Teismann P: **MPP(+)-induced toxicity in the presence of**  
1211 **dopamine is mediated by COX-2 through oxidative stress.** *Naunyn Schmiedebergs*  
1212 *Arch Pharmacol* 2011, **384**:157-167.
- 1213 114. Kwon S, Iba M, Masliah E, Kim C: **Targeting Microglial and Neuronal Toll-like**  
1214 **Receptor 2 in Synucleinopathies.** *Exp Neurobiol* 2019, **28**:547-553.
- 1215 115. Doorn KJ, Moors T, Drukarch B, van de Berg W, Lucassen PJ, van Dam AM:  
1216 **Microglial phenotypes and toll-like receptor 2 in the substantia nigra and**  
1217 **hippocampus of incidental Lewy body disease cases and Parkinson's disease**  
1218 **patients.** *Acta Neuropathol Commun* 2014, **2**:90.
- 1219

## 1220 **Figure and table legends**

1221

1222 **Figure 1.** Intrastriatal injection of murine  $\alpha$ -syn PFFs induced  $\alpha$ -syn inclusions in various  
1223 brain regions. Mice were euthanized 90 days after injection (90 dpi, n=10-11/group). A.  
1224 PhosphoSER129  $\alpha$ -syn immunostaining showed numerous  $\alpha$ -syn inclusions in neuritic and  
1225 neuronal body structures in different brain regions. Widespread  $\alpha$ -syn inclusions were  
1226 observed bilaterally in frontal cortex and the amygdala, ipsilaterally in the striatum and the  
1227 Substantia Nigra (SN), and only minimally in the contralateral striatum and SN. None were  
1228 observed in the hippocampus. No inclusions were observed in either side of the brains of  
1229 PBS-injected control mice. Pictures show the ipsilateral side of these mice. B. Proteinase-K  
1230 digestion on thin sections generated from paraffin-embedded tissue blocks revealed the  
1231 presence of digestion-resistant  $\alpha$ -syn inclusions stained for PhosphoSER129  $\alpha$ -syn. Shown  
1232 here are ipsilateral striatum and amygdala for illustration. C. Proximity-ligation assay using a

1233 monoclonal PhosphoSER129  $\alpha$ -syn antibody showed the presence of enhanced levels of  
1234 oligomeric forms of  $\alpha$ -syn in the hippocampus of PFF-injected mice, where no inclusions  
1235 could be detected 90 dpi, compared to PBS-injected controls. Scale bar = 250  $\mu$ m (A), 250  
1236  $\mu$ m (B), 25  $\mu$ m (C).

1237

1238 **Figure 2.** Intrastriatal injection of murine  $\alpha$ -syn PFFs induced neurodegeneration in various  
1239 brain regions. Mice were euthanized 90 dpi. In the frontal cortex and the hippocampus, a  
1240 significant bilateral loss of synaptophysin-positive presynaptic terminals was observed (first  
1241 two rows). In the striatum, a significant ipsilateral loss of TH-positive axonal fibers and  
1242 DAT-positive synaptic terminals was observed (3<sup>rd</sup> and 4<sup>th</sup> row). In the SN, a significant loss  
1243 of TH-positive neurons was observed only ipsilaterally. For group comparisons and graphing,  
1244 ipsilateral PBS measures were combined contralateral PBS measures, since they were similar.  
1245 Pictures show the ipsilateral side of PBS-injected mice. \*\*\*\* p<0.0001, \*\* p<0.01, compared  
1246 to PBS controls by Dunnett's post-hoc; n = 10-11/group. Scale bars: 18  $\mu$ m (for frontal  
1247 cortical and hippocampal synaptophysin panels), 22.5  $\mu$ m (for striatal TH and DAT panels),  
1248 80  $\mu$ m (for Subst. Nigra panels)

1249

1250 **Figure 3.** Intrastriatal injection of murine  $\alpha$ -syn PFFs induced widespread microgliosis in  
1251 different brain regions. Mice were euthanized 90 dpi. Panels show microgliosis measured on  
1252 Iba1-stained sections of frontal cortex (upper row), hippocampus (second row), striatum (3<sup>rd</sup>  
1253 row), and Subst. Nigra (last row), and on CD68-stained sections of striatum (4<sup>th</sup> row). A very  
1254 strong microgliosis (up to 4x over control) was observed bilaterally in frontal cortex,  
1255 hippocampus, and SN. No increase in Iba1 signal, but a significant bilateral increase in CD68  
1256 signal was observed in the striatum of PFF-injected mice. For group comparisons and  
1257 graphing, ipsilateral PBS measures were combined contralateral PBS measures, since they

1258 were similar. Pictures show the ipsilateral side of PBS-injected mice. \*\*\*\* p<0.0001, \*  
1259 p<0.05, compared to PBS controls by Dunnett's post-hoc; n = 10-11/group. Scale bars: 22.5  
1260  $\mu\text{m}$  (for all panels).

1261

1262 **Figure 4.** Different PD-related pathologies in the brains of mice injected intrastrially with  
1263  $\alpha$ -syn PFFs do not correlate with each other. Mice were euthanized 90 dpi. A.  $\alpha$ -syn  
1264 inclusion load did not correlate with neurodegeneration (loss TH-positive neurons, A1) or  
1265 with microgliosis (A2) in the SN (Nigra), nor with neurodegeneration (loss of synaptophysin-  
1266 positive synaptic terminals, A3) or with microgliosis (A4) in the frontal cortex (Cortex). B.  
1267 Microgliosis did not correlate with loss of TH-positive neurons in the SN after intrastriatal  
1268 PFF injection, but did so after intrastriatal injection of the toxin 6-OHDA. The microgliosis,  
1269 measured on Iba1-stained section, was also much higher in the Subst. Nigra of PFF-injected  
1270 mice than in that of 6-OHDA-injected mice.

1271 All measures shown are from the ipsilateral brain sides; similar observations were made for  
1272 the contralateral sides of PFF-injected mice. Correlation analyses were done using Spearman  
1273 rank test for data set including  $\alpha$ -syn inclusion load measures, and with Pearson's test for  
1274 data sets with the other measures.

1275

1276 **Figure 5:** Strong microglial response after intrastriatal injection of  $\alpha$ -syn oligomers.  
1277 Oligomers were prepared and injections were performed as described in Materials and  
1278 Methods. A strong microgliosis was observed in different brain regions 13 dpi, showing that  
1279  $\alpha$ -syn oligomers are robust microglial activators in vivo. Scale bar = 40  $\mu\text{m}$ .

1280

1281 **Figure 6.** Differentially expressed genes induced in the ipsilateral ventral midbrain of mice at  
1282 13 dpi (A) and 90 dpi (B) after intrastriatal injections of  $\alpha$ -syn PFFs. Comparisons for each

1283 time point were made between gene expressed in ipsilateral ventral midbrain of PFF-injected  
1284 mice versus those in the ipsilateral ventral midbrain for PBS-injected mice (ipsi PFF vs. ipsi  
1285 PBS, n =6/group; upper 4 panels), and between gene expressed in ipsilateral ventral midbrain  
1286 versus the contralateral ventral midbrains of PFF-injected mice (ipsi PFF vs. contra PFF, n  
1287 =6/group; lower 4 panels). Panels on the left show Venn diagrams with numbers of DEGs  
1288 with a significance level of  $p < 0.05$  (n=6 mice/group). Because some gene products have an  
1289 effect within biological pathways while the expression of their genes may only change  
1290 minimally, we show DEGs that emerge with this level of statistical stringency. In ipsi PFF vs.  
1291 ipsi PBS, the number of DEGs was 2631 at 13 DPI, and 2584 at 90 DPI, with 985 DEGs  
1292 common to both time points. In ipsi PFF vs. contra PFF, the number of DEGs was 3477 at 13  
1293 DPI, and 3209 at 90 DPI, with 1356 DEGs common to both time points. Panels on the right  
1294 show Venn diagrams with the number of DEGs after adjusting for multiple hypothesis testing  
1295 at  $p < 0.1$ . In ipsi PFF vs. ipsi PBS, the number of DEGs was 266 at 13 DPI, and 82 at 90  
1296 DPI, with 39 DEGs common to both time points. In ipsi PFF vs. contra PFF, the number of  
1297 DEGs was 648 at 13 DPI, and 588 at 90 DPI, with 227 DEGs common to both time points.  
1298 The Venn diagrams below the main ones indicate the number of DEGs that show enhanced  
1299 (“up”) versus decreased (“down”), as well as the overlaps, in the different comparisons.

1300

1301 **Figure 7.** Enriched inflammatory pathways precedes neurodegeneration in mouse ventral  
1302 midbrains after intrastriatal  $\alpha$ -syn PFFs injection. Enrichment map of gene expression  
1303 profiles were derived from GSEA. Statistics were done by weighted Kolmogorov-Smirnov,  
1304 gene set size limits were set to min15 – max250. Details of curation procedure used to group  
1305 BPs (represented as dots, either red if upregulated, or blue if downregulated) into high-level  
1306 functional gene set clusters of BPs of related biological function are described in Material &  
1307 Methods. At 13 dpi, comparing ipsi PFF to either ipsi PBS or contra PFF, most BPs were



1308 upregulated and associated with gene sets related to immune and inflammation processes.  
1309 This shows that, in the ipsilateral nigro-striatum, neuroinflammation precedes  
1310 neurodegeneration (measurable at 90 dpi), and might contribute to its development. At 90  
1311 dpi, comparing ipsi PFF to ipsi PBS, all BPs, including those associated with inflammation  
1312 gene sets, were downregulated, possibly reflecting the neurodegenerative process itself.  
1313 Comparing ipsi PFF to contra PFF at this time point, most BPs were upregulated.

1314

1315 **Figure 8.** Top 20 DEGs in mouse ventral midbrain after intrastriatal injection of  $\alpha$ -syn PFF  
1316 indicate involvement of microglia in initial pathological events. Cellular source of DEGs was  
1317 determined using the brain RNAseq database: <https://www.brainrnaseq.org/>. The top panels  
1318 show pie charts with the cellular source of the 20 top DEGs when comparing ipsi PFF to ipsi  
1319 PBS (left panels) or ipsi PFF with contra PFF (right panels) at 13 dpi and 90 dpi. At 13 dpi,  
1320 comparing ipsi PFF with ipsi PBS or contra PFF, 45% and 40%, respectively, of the top 20  
1321 DEGs were microglial. At 90 dpi, comparing ipsi PFF with ipsi PBS, 50% of top 20 DEGs  
1322 were neuronal, possibly a reflection of neurodegeneration. The bottom panel lists the gene  
1323 products of the gene symbols, coded proteins, the associated cell type 20, the fold change  
1324 (FC) and the pff of all top 20 DEGs for each comparison.

1325

1326 **Table 1: Unique molecular features of microglial response to intrastriatal  $\alpha$ -syn PFF**  
1327 **injection.**

1328 Table shows genes and their coded proteins for factors typically associated with microglial  
1329 pro-inflammatory M1 profile (highlighted in yellow), for factors typically associated with  
1330 microglial anti-inflammatory M2 profile (highlighted in green), and for generic microglial  
1331 activation factors (highlighted in blue). Comparisons are between ventral midbrains of ipsi  
1332 PFF *versus* ipsi PBS and of ipsi PFF *versus* contra PFF. The rank p-values and the FDRs are

1333 given. The proteins whose genes have either a significant p-value (<0.05) or pfp < 0.1 are  
1334 highlighted in bold. Already at 13 dpi, *Cybb*, the gene for NADPH oxidase 2, a mediator of  
1335 oxidative stress, was upregulated in ipsi PFF midbrain, a region that showed  
1336 neurodegeneration at 90 dpi (see above). Another gene, *Ptgs2*, whose product,  
1337 cyclooxygenase 2, has been reported to generate neurotoxic arachidonic acid metabolites,  
1338 was also upregulated in ipsi PFF midbrains, most strongly so (pfp <0.1) when comparing ipsi  
1339 PFF with contra PFF. This gene can be expressed also in astrocytes. *Cd68*, whose protein is  
1340 linked to lysosomal function and possibly acts as a scavenger receptor, was also strongly  
1341 upregulated in ipsi PFF midbrains. Finally, a triad of factors associated with microglia  
1342 activation (*Tyrobp*, *Trem2*, *Tlr2*) was upregulated at 13 dpi in ipsi PFF midbrains. Their  
1343 downregulation at 90 dpi in ipsi PFF versus ipsi PBS could indicate that the inflammation  
1344 process starts to resolve.

1345

1346

#### 1347 **Supplemental figures and tables legends**

1348

1349 **Suppl. fig.1:** Western blot characterization of  $\alpha$ -syn moieties used for intrastriatal injections.  
1350 Loading of the gel was as follows: lanes 1, 6, 14 – ladder; lanes 5, 10,11- blank; lanes 2,3,4 –  
1351  $\alpha$ -syn oligomer, 10, 100, and 500 ng respectively; lanes 7, 8, 9 –  $\alpha$ -syn PFFs, not sonicated,  
1352 10,100, 500 ng respectively; lanes 11, 12, 13 –  $\alpha$ -syn PFFs (sonicated), 10,100, 500 ng  
1353 respectively. Bands from corresponding to the MW of  $\alpha$ -syn monomers, dimers, and trimers  
1354 are circled (red, blue, orange, respectively). Note the presence of high molecular weight  
1355 moieties (visible as a smear) after loading of non-sonicated PFFs. The sonication process of  
1356 PFFs appears to reduce all higher molecular weight species of  $\alpha$ -syn and the amount of

1357 dimers and monomers, since smears and monomer/dimer bands were visible after loading  
1358 100 ng of non-sonicated PFFs, but not after loading the same amount of sonicated PFFs.

1359

1360 **Suppl. fig. 2:** Minimal presence of  $\alpha$ -syn inclusions in different brain regions 13 DPI after  
1361 intrastriatal injection of  $\alpha$ -syn PFFs. Only few  $\alpha$ -syn inclusions were seen, ipsi- and  
1362 contralaterally, in the frontal cortex, amygdala, and ipsilaterally, but not contralaterally, in  
1363 the striatum and SN. Scale bar = 130  $\mu$ m.

1364

1365 **Suppl. Fig. 3:** No nigro-striatal degeneration and microgliosis 13 dpi after intrastriatal  
1366 injection of  $\alpha$ -syn PFFs. No loss of striatal TH-positive axons (first row), striatal DAT-  
1367 positive synaptic terminals (second row), nigral TH-positive neurons (third row) was  
1368 observed 13 dpi after injection of PFFs. No increase of Iba1-positive microglial reaction in  
1369 the SN was observed (last row). Microphotographs show examples of PBS-injected control  
1370 brains (ipsilateral) and ipsilateral  $\alpha$ -syn PFF-injected brains. Scale bars = 25  $\mu$ m (striatal  
1371 panels), 200  $\mu$ m (Subst. Nigra panels).

1372

1373 **Suppl. fig. 4:** Heatmaps illustrating the ventral midbrain gene expression patterns at 13 dpi  
1374 and 90 dpi after intrastriatal injection of  $\alpha$ -syn PFFs. Heatmaps are shown for p-values < 0.05  
1375 or pfp < 0.1. Scaled row expression values (row Z-score) in red indicate higher, in blue lower,  
1376 and in white unchanged gene expression (see Materials and Methods for details).  
1377 Comparisons of ipsi PFF *versus* ipsi PBS (upper panel row) and ipsi PBS *versus* contra PFF  
1378 (lower panel row) reveal distinctive gene expression patterns at 13 dpi for both comparisons  
1379 (whether higher, pfp < 0.1, or lower, p < 0.05, statistical stringency is used), whereas a  
1380 distinctive patterns at 90 dpi only appears in the ipsi PFF *versus* contra PFF, but not in the  
1381 ipsi PFF *versus* ipsi PBS, comparisons.

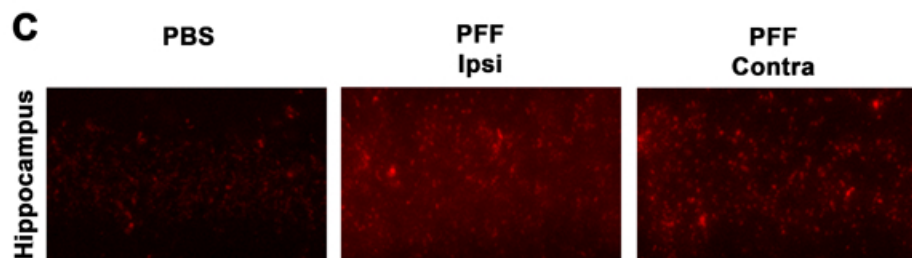
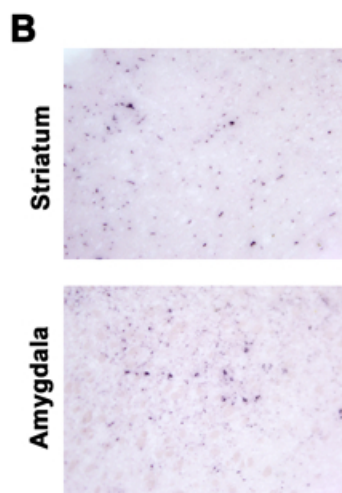
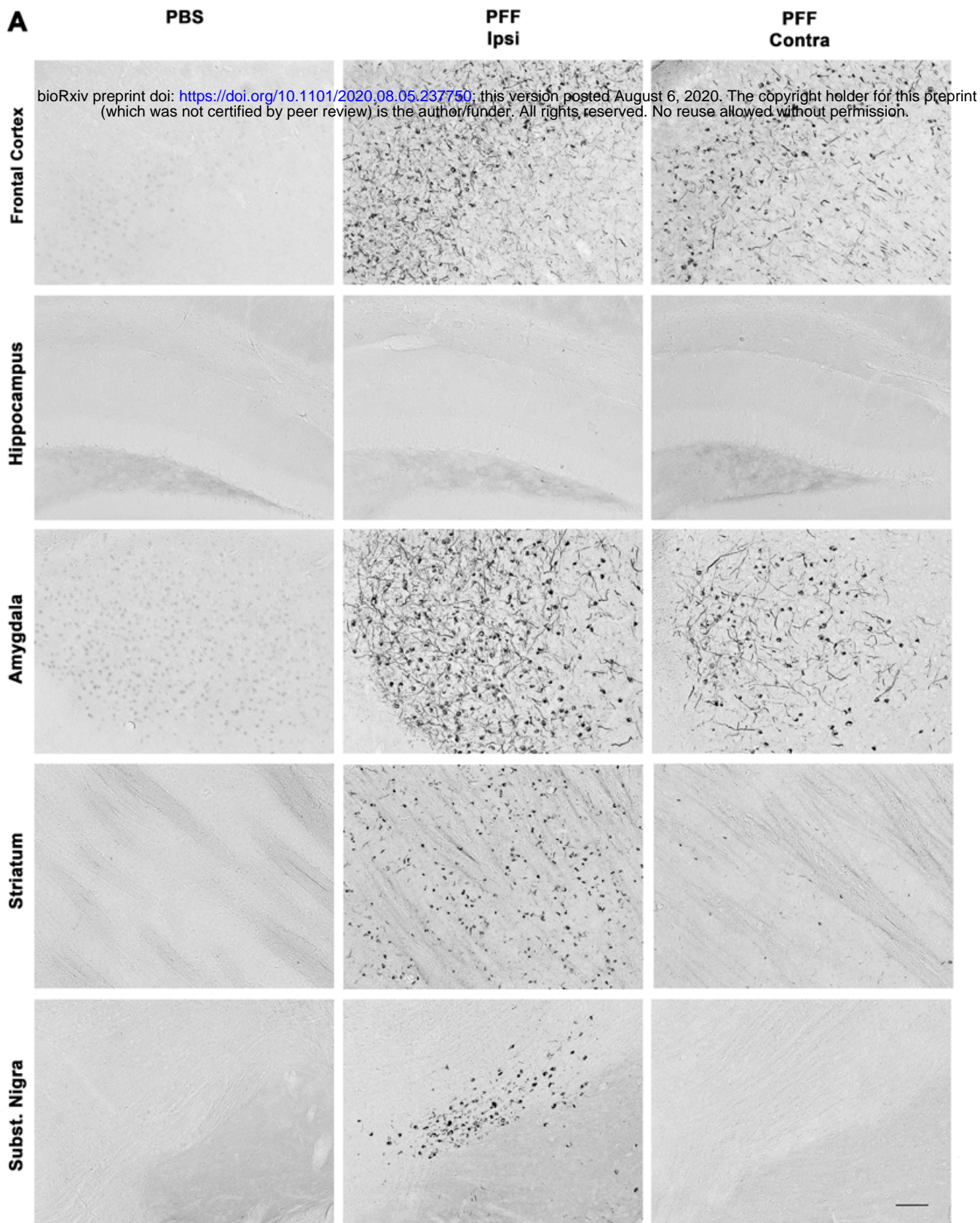
1382

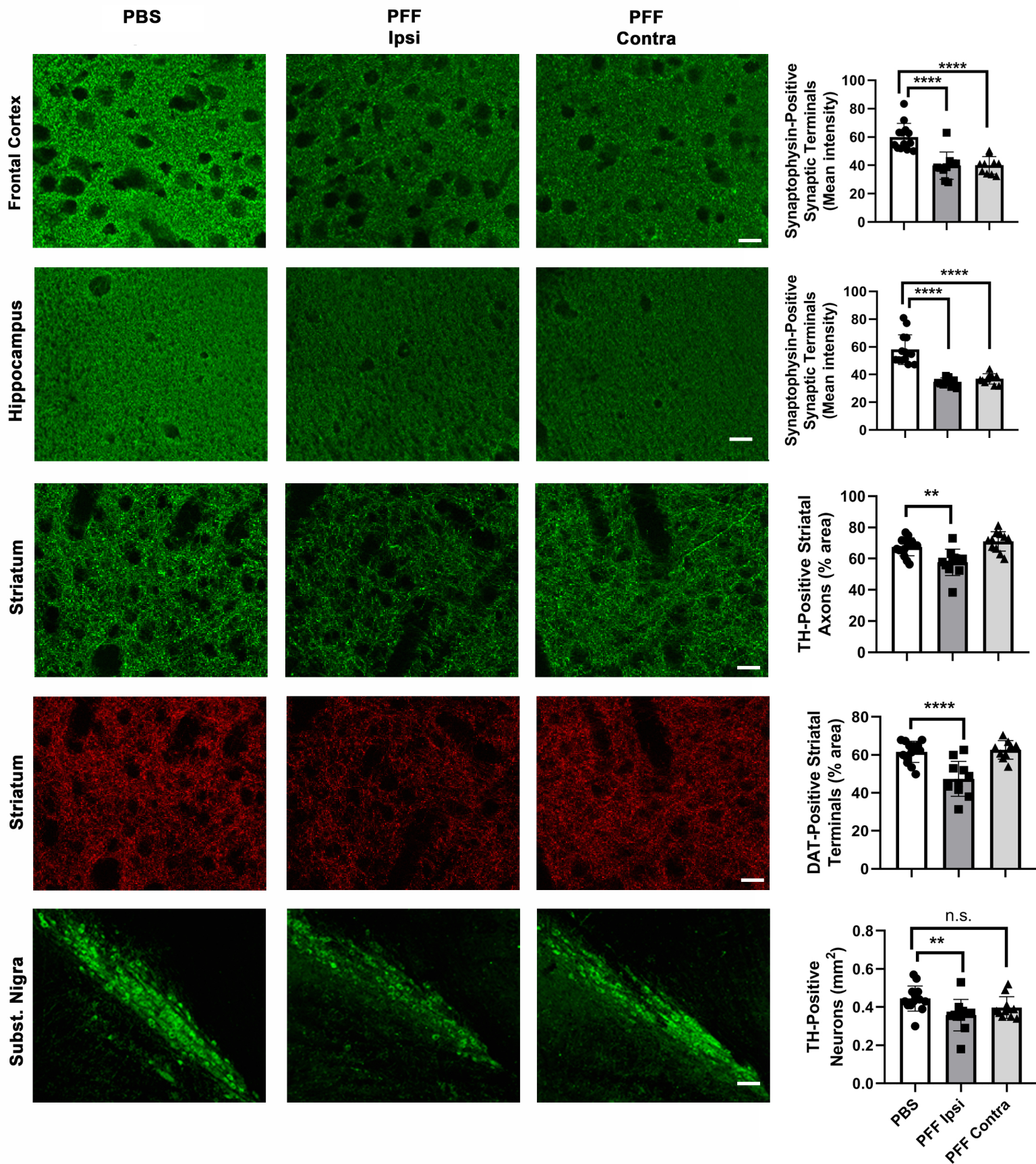
1383 *Supplemental tables legends*

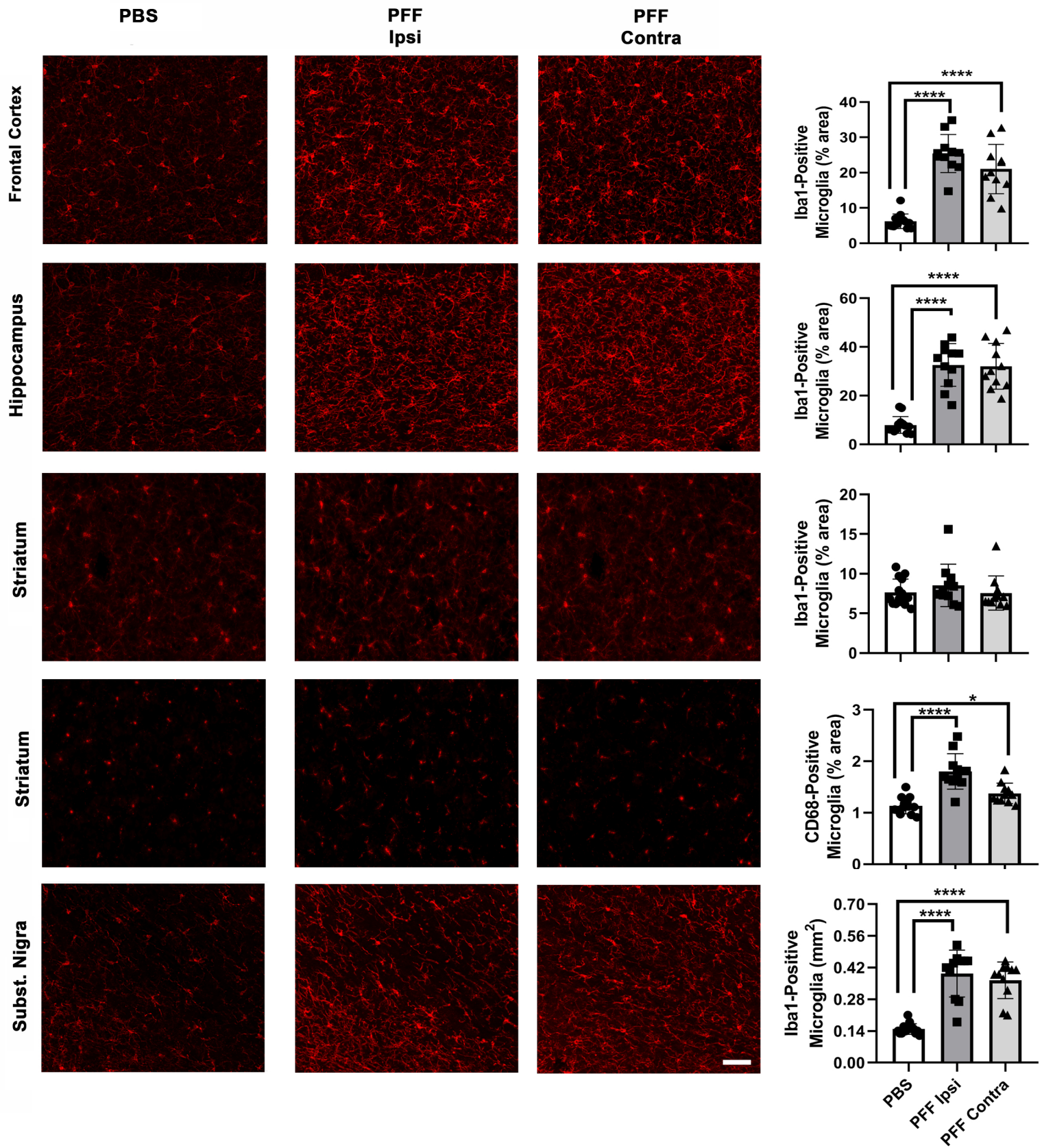
1384 **Suppl table 1: Antibodies used in this study**

1385 **Suppl table 2: Softwares used in this study**

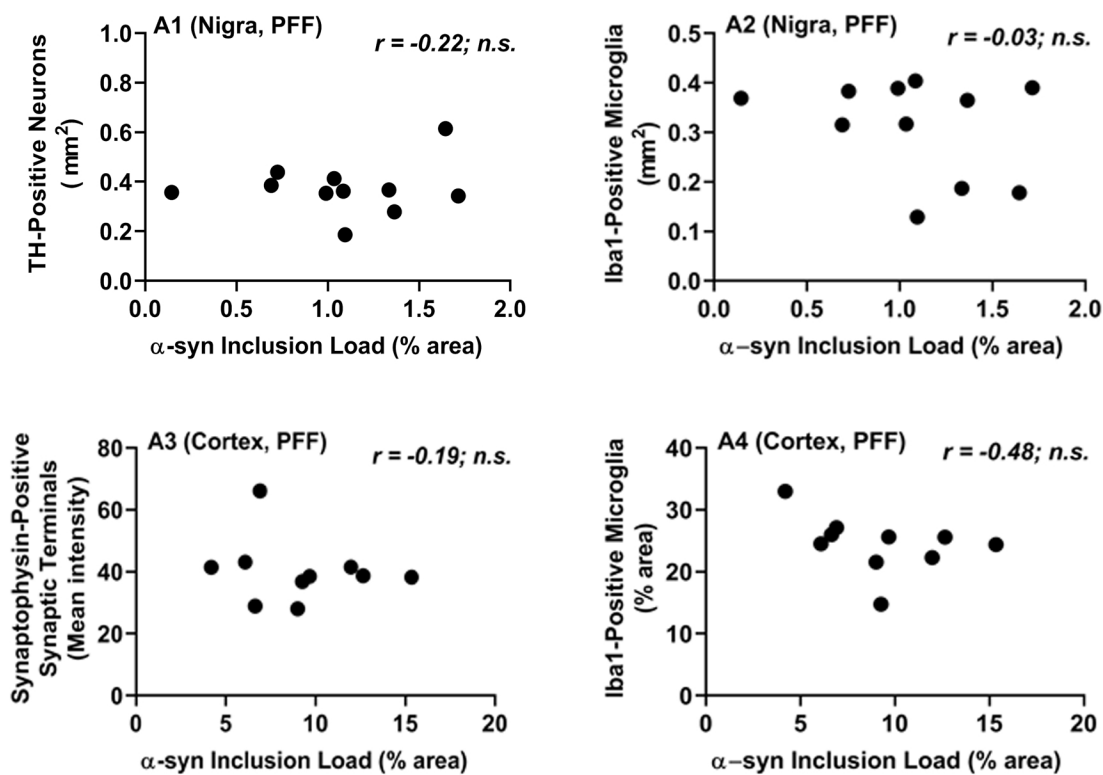
1386 **Suppl table 3: Molecular astrocyte and peripheral immune cell markers**



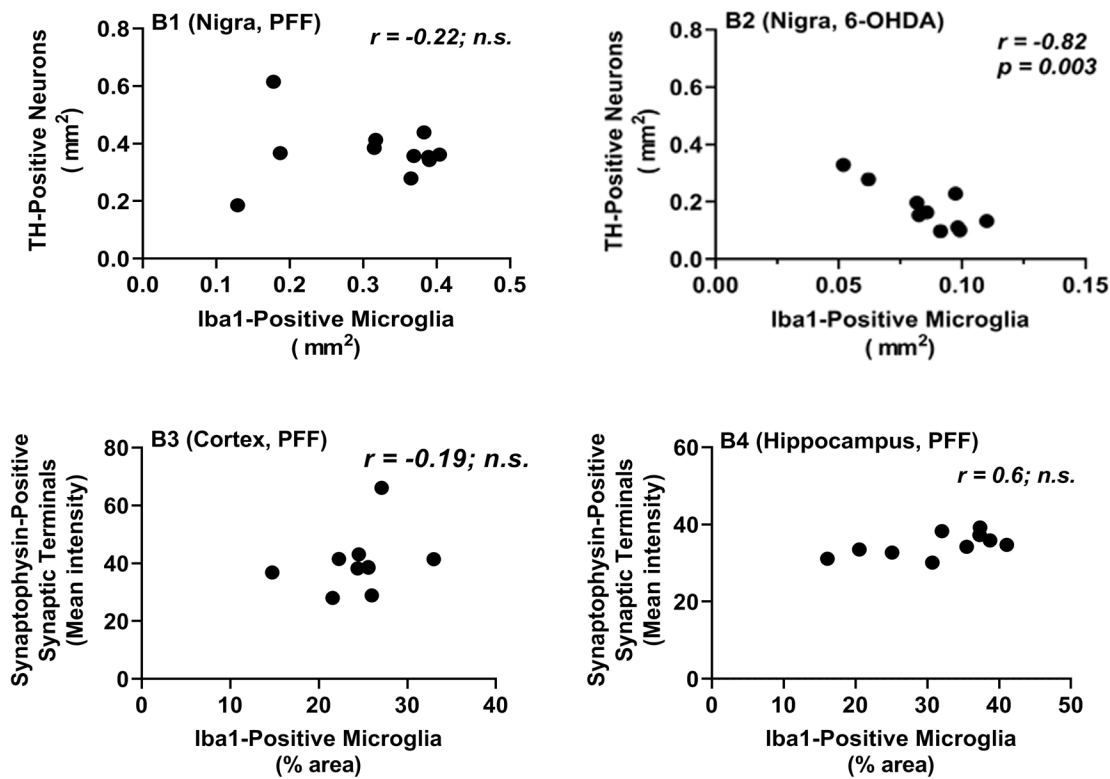




**A**



**B**

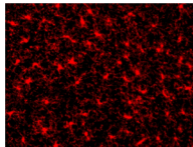
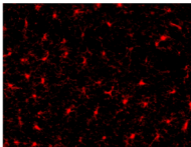




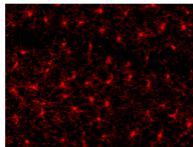
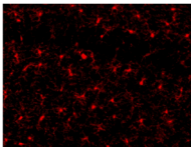
Vehicle

$\alpha$ -Syn Oligomers

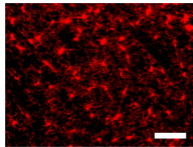
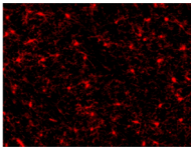
Frontal Cortex



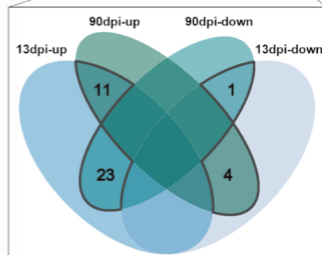
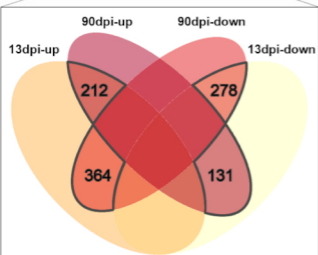
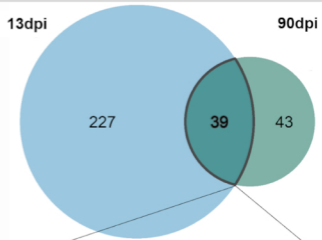
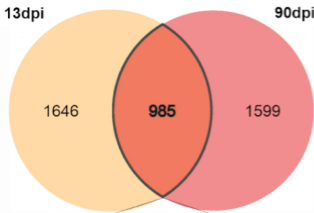
Hippocampus



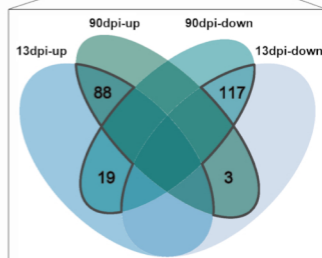
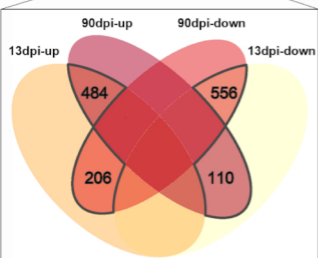
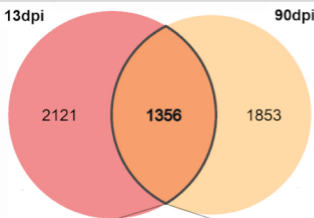
Striatum



### ipsi PFF vs ipsi PBS



### ipsi PFF vs contra PFF

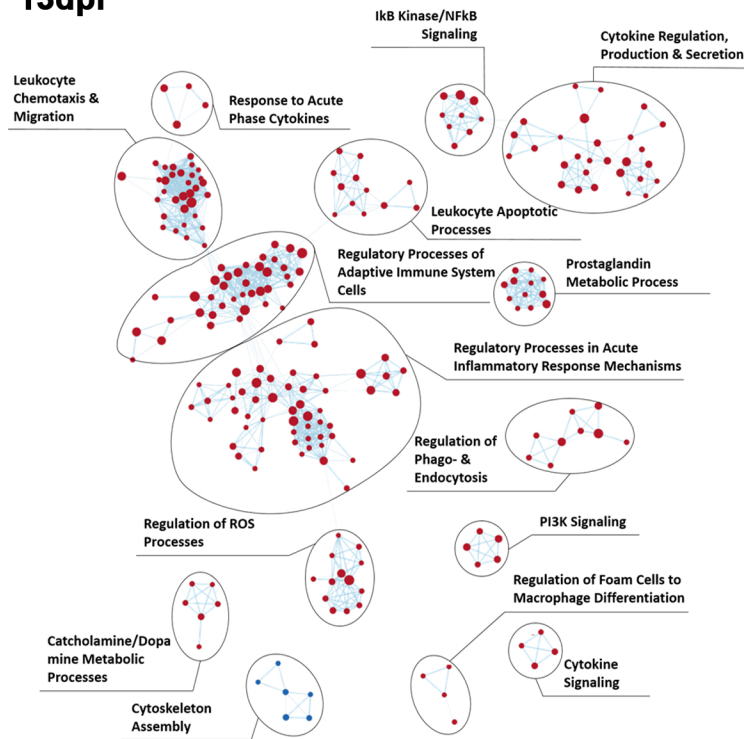


$P < 0.05$

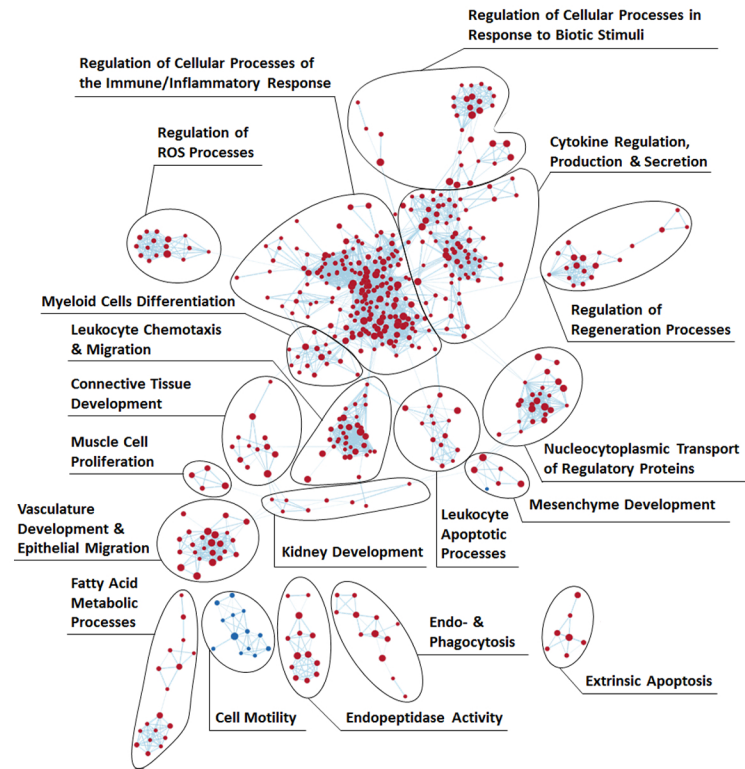
$P_{fp} < 0.1$

# ipsi PFF versus ipsi PBS

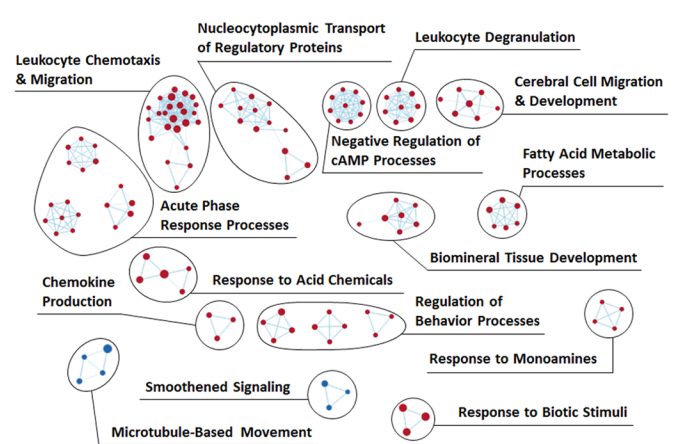
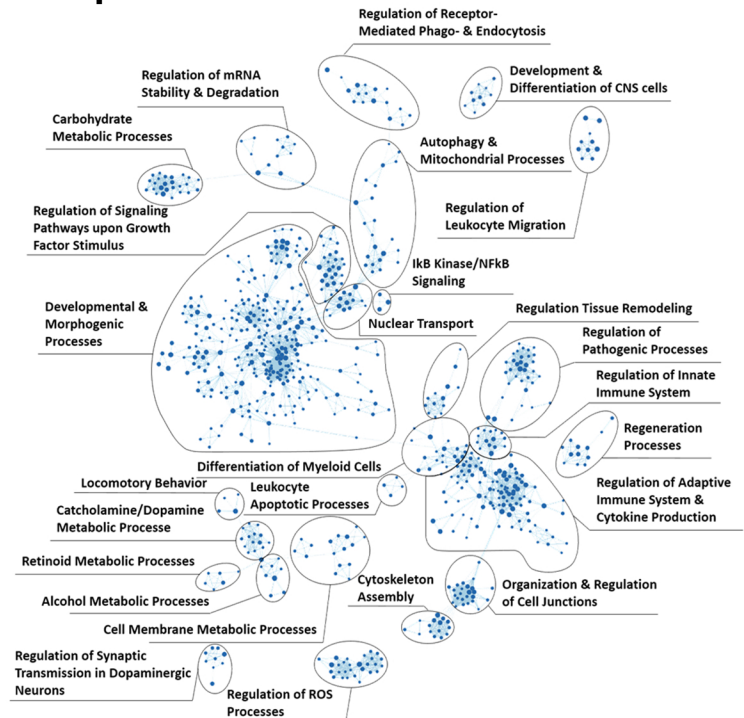
13dpi



# ipsi PFF versus contra PFF



90dpi

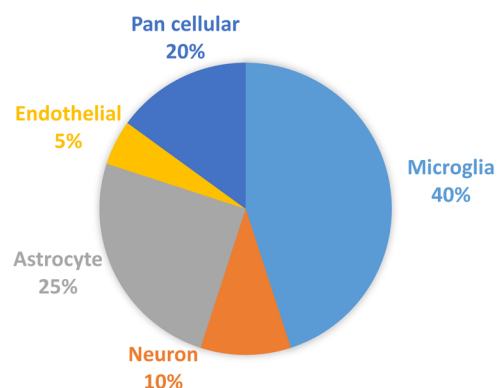
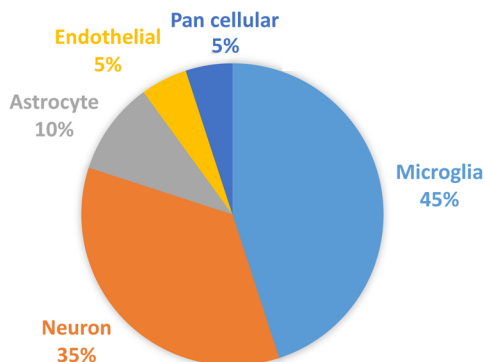


**A**

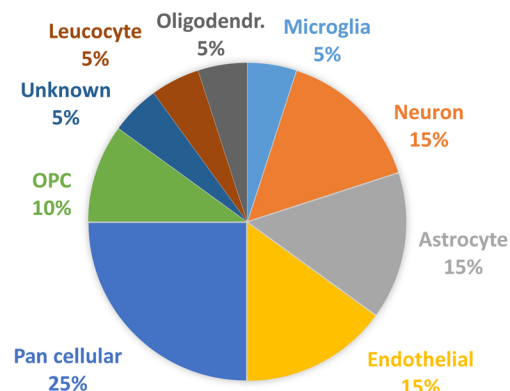
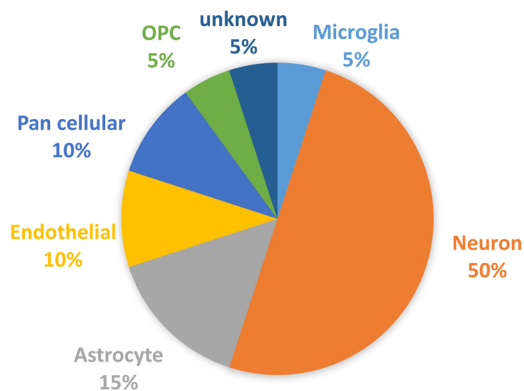
**ipsi PFF versus ipsi PBS**

**ipsi PFF versus contra PFF**

**13 dpi**



**90 dpi**



**B**

Gene Symbol	Protein Name	Cell type	FC	Pfp	Gene Symbol	Protein Name	Cell type	FC	Pfp
<b>13dpi - ipsi PFF versus ipsi PBS</b>					<b>13dpi - ipsi PFF versus contra PFF</b>				
<i>Slc6a3</i>	Sodium-dependent dopamine transporter	Neuron	2.600	2.94E-08	<i>Oxt</i>	Oxytocin	Pan cellular	-2.762	2.97E-13
<i>Oxt</i>	Oxytocin	Pan cellular	-1.519	1.64E-06	<i>Slc6a3</i>	Sodium-dependent dopamine transporter	Neuron	2.749	5.55E-10
<i>Lilrb4a</i>	Leukocyte immunoglobulin-like receptor, subfamily B, member 4A	Microglia	2.074	3.59E-06	<i>Tmem212</i>	Transmembrane protein 212	Astrocyte	-2.203	1.98E-09
<i>Spp1</i>	Osteopontin	Microglia	1.921	9.29E-06	<i>Stom13</i>	Stomatin-like protein 3	Pan cellular	-2.211	1.99E-09
<i>Cst7</i>	Cystatin F (leukocystatin)	Microglia	1.921	1.63E-05	<i>Lilrb4a</i>	Leukocyte immunoglobulin-like receptor, subfamily B, 4A	Microglia	2.437	2.18E-09
<i>Lpl</i>	Lipoprotein lipase	Microglia	1.795	1.70E-05	<i>Cst7</i>	Cystatin F (leukocystatin)	Microglia	2.412	3.46E-09
<i>Ccl3</i>	Chemokine (C-C motif) ligand 3	Microglia	1.819	1.72E-05	<i>Ogn</i>	Osteoglycin	Endothelial	2.296	4.44E-09
<i>Plin4</i>	Perilipin 4	Neuron	1.747	5.44E-05	<i>Clec7a</i>	C-type lectin domain family 7 member A	Microglia	2.348	8.01E-09
<i>Clec7a</i>	C-type lectin domain family 7 member A	Microglia	1.808	5.94E-05	<i>Ak7</i>	Adenylate kinase 7	Astrocyte	-2.112	8.52E-09
<i>Ogn</i>	Osteoglycin	Endothelial	1.753	8.19E-05	<i>Spp1</i>	Osteopontin	Microglia	2.232	1.28E-08
<i>Avp</i>	Arginine vasopressin	Neuron	-1.149	1.30E-04	<i>Ccl3</i>	Chemokine (C-C motif) ligand 3	Microglia	2.367	1.33E-08
<i>Prg4</i>	Proteoglycan 4 (lubricin)	Astrocyte	1.777	1.72E-04	<i>Trh</i>	Thyrotropin releasing hormone	Astrocyte	-2.067	2.72E-08
<i>Gfap</i>	Glial fibrillary acidic protein	Astrocyte	1.633	1.85E-04	<i>Cdhr3</i>	Cadherin-related family member 3	Pan cellular	-1.996	5.01E-08
<i>Sim1</i>	Single-minded homolog 1	Neuron	-1.643	1.88E-04	<i>Slc17a7</i>	Vesicular glutamate transporter 1	Pan-cellular	2.288	1.10E-07
<i>Sgk1</i>	Serum/glucocorticoid regulated kinase 1	Microglia	1.675	2.00E-04	<i>Cd68</i>	CD68 antigen	Microglia	2.042	1.31E-07
<i>Cd68</i>	CD68 antigen	Microglia	1.683	2.07E-04	<i>Ccl6</i>	Chemokine (C-C motif) ligand 6	Microglia	1.980	1.96E-06
<i>Chrna6</i>	Neuronal acetylcholine receptor subunit alpha-6	Neuron	1.585	2.11E-04	<i>Prg4</i>	Proteoglycan 4 (lubricin)	Astrocyte	1.999	1.99E-06
<i>Zbtb16</i>	Zinc finger and BTB domain containing 16	Neuron	1.644	2.73E-04	<i>Dynlrb2</i>	Dynein light chain roadblock-type 2	Astrocyte	-1.815	2.40E-06
<i>Tyrobp</i>	TYRO protein tyrosine kinase binding protein	Microglia	1.628	3.48E-04	<i>Fam183b</i>	Protein FAM183B	Neuron	-1.889	4.02E-06
<i>Fezf1</i>	Fez family zinc finger protein 1	Neuron	-1.475	3.74E-04	<i>Ccl9</i>	Chemokine (C-C motif) ligand 9	Microglia	1.838	7.89E-06
<b>90dpi - ipsi PFF versus ipsi PBS</b>					<b>90dpi - ipsi PFF versus contra PFF</b>				
<i>Slc6a3</i>	Sodium-dependent dopamine transporter	Neuron	-2.383	1.51E-06	<i>Kcnj13</i>	Inward rectifier potassium channel 13	Pan cellular	2.556	7.66E-09
<i>Gh</i>	Growth hormone	Endothelial	2.007	1.09E-05	<i>Prg4</i>	Proteoglycan 4 (lubricin)	Astrocyte	2.593	1.03E-08
<i>Th</i>	Tyrosine hydroxylase	Neuron	-1.874	5.40E-04	<i>Ogn</i>	Osteoglycin	Endothelial	2.749	1.15E-08
<i>Slc18a2</i>	Synaptic vesicular amine transporter	Neuron	-1.782	1.33E-03	<i>Slc13a4</i>	Solute carrier family 13 (Sodium/sulfate symporter), member 4	OPC	2.330	4.82E-07
<i>Chrn3</i>	Neuronal acetylcholine receptor subunit beta-3	Neuron	-1.748	3.72E-03	<i>Ranbp3l</i>	RAN binding protein 3-like	Astrocyte	2.334	4.89E-07
<i>Slc5a7</i>	High affinity choline transporter 1	Neuron	1.630	3.95E-03	<i>Crym</i>	Ketimine reductase mu-crystallin	Pan cellular	2.193	1.06E-06
<i>Cyr61</i>	Cysteine-rich angiogenic inducer 61	Astrocyte	-1.692	4.44E-03	<i>Col6a1</i>	Collagen alpha-1(VI) chain	Neuron	2.115	1.41E-06
<i>Gm10754</i>	Unnamed protein	Neuron	1.364	5.64E-03	<i>Rgs16</i>	Regulator of G-protein signaling 16	Endothelial	-2.062	1.61E-06
<i>Taf1d</i>	TATA box-binding protein-associated factor RNA polymerase I	Endothelial	1.560	7.33E-03	<i>Slitrk6</i>	SLIT and NTRK-like protein 6	OPC	-2.139	1.91E-06
<i>Chrna6</i>	Neuronal acetylcholine receptor subunit alpha-6	Neuron	-1.707	7.61E-03	<i>Stom13</i>	Stomatin-like protein 3	Pan cellular	-2.146	1.95E-06
<i>Kcnj13</i>	Inward rectifier potassium channel 13	Pan cellular	-1.556	1.38E-02	<i>C030013G03Rik</i>	Unknown	unknown	-2.018	2.12E-06
<i>Ret</i>	Proto-oncogene tyrosine-protein kinase receptor Ret	Neuron	-1.602	1.43E-02	<i>Car12</i>	Carbonic anhydrase 12	Neuron	2.151	2.28E-06
<i>Meis2</i>	Homeobox protein Meis2	Neuron	1.434	1.43E-02	<i>Pomc</i>	Pro-opiomelanocortin-alpha	Endothelial	-2.112	3.09E-06
<i>Slc13a4</i>	Solute carrier family 13 (Sodium/sulfate symporter), member 4	OPC	-1.358	1.56E-02	<i>Tcf7l2</i>	Transcription factor 7-like 2	Oligodendr.	-1.996	3.73E-06
<i>Ranbp3l</i>	RAN binding protein 3-like	Astrocyte	-1.288	2.13E-02	<i>Omd</i>	Osteomodulin	Astrocyte	2.155	4.48E-06
<i>Mir5098</i>	Stem-loop RNA, non coding	Pan cellular	1.507	2.13E-02	<i>Osr1</i>	Protein odd-skipped-related 1	Pan cellular	1.998	1.43E-05
<i>Aldh1a2</i>	Aldehyde dehydrogenase family 1, member A2	Neuron	-1.442	2.16E-02	<i>Nov</i>	Protein NOV homolog	Neuron	2.039	1.51E-05
<i>Trh</i>	Thyrotropin releasing hormone	Astrocyte	1.436	2.34E-02	<i>Trav7d-4</i>	T cell receptor alpha variable 7D-4	Leucocyte*	-1.783	1.69E-05
<i>C030013G03Rik</i>	Unknown	unknown	-1.540	2.36E-02	<i>Cox6a2</i>	Cytochrome c oxidase subunit 6A2, mitochondrial	Microglia	-1.837	1.73E-05
<i>Prkcd</i>	Protein kinase C delta type	Microglia	-1.368	2.45E-02	<i>Oxt</i>	Oxytocin	Pan cellular	-1.835	1.85E-05

Gene Symbol	Protein	ipsi PFF versus ipsi PBS						ipsi PFF versus contra PFF					
		13dpi			90dpi			13dpi			90dpi		
		FC	p-Value	Pfp	FC	p-Value	Pfp	FC	p-Value	FDR	FC	p-Value	Pfp
<i>Cybb</i>	NAPDH oxidase 2	1.407	<b>5.17E-05</b>	<b>2.24E-02</b>	-1.221	<b>5.36E-03</b>	3.95E-01	1.413	<b>1.09E-04</b>	<b>2.06E-02</b>	1.155	7.08E-02	7.60E-01
<i>Ptgs2</i>	Cyclooxygenase 2	1.285	<b>1.50E-03</b>	1.74E-01	-1.189	<b>1.18E-03</b>	2.06E-01	1.506	<b>1.28E-05</b>	<b>4.52E-03</b>	1.436	<b>8.06E-05</b>	<b>1.84E-02</b>
<i>Cxcl10</i>	Chemokine (C-X-C motif) ligand 10	1.226	<b>6.11E-03</b>	3.62E-01	-1.141	1.03E-01	9.28E-01	1.344	<b>7.64E-04</b>	<b>7.62E-02</b>	-1.003	5.15E-01	1.10E+00
<i>Cd86</i>	CD86 antigen	1.112	8.32E-02	9.65E-01	-1.139	5.96E-02	8.08E-01	1.304	<b>2.08E-03</b>	1.38E-01	1.073	1.87E-01	9.36E-01
<i>Il1b</i>	Interleukin 1 beta	1.131	8.25E-02	9.62E-01	1.071	3.38E-01	1.04E+00	1.085	2.54E-01	1.06E+00	1.091	2.41E-01	9.72E-01
<i>Il6</i>	Interleukin 6	1.030	4.26E-01	1.07E+00	-1.022	4.75E-01	1.07E+00	1.032	4.48E-01	1.09E+00	-1.050	3.33E-01	1.06E+00
<i>Tnf</i>	Tumor necrosis factor alpha	-1.003	6.35E-01	1.02E+00	1.002	6.81E-01	9.97E-01	1.017	4.93E-01	1.08E+00	1.082	3.04E-01	1.00E+00
<i>Ccl2</i>	Chemokine (C-C motif) ligand 2	-1.023	3.86E-01	1.07E+00	-1.073	1.92E-01	1.03E+00	-1.050	2.35E-01	1.06E+00	1.082	1.46E-01	9.10E-01
<i>Nos2</i>	Nitric oxide synthase 2, inducible	1.069	2.86E-01	1.10E+00	-1.063	3.21E-01	1.06E+00	-1.014	6.54E-01	1.05E+00	-1.003	6.12E-01	1.10E+00
<i>Il12b</i>	Interleukin 12b	1.003	6.24E-01	1.03E+00	-1.023	5.26E-01	1.06E+00	-1.006	6.11E-01	1.06E+00	1.074	3.31E-01	1.01E+00
<i>Il12a</i>	Interleukin 12a	-1.042	4.72E-01	1.06E+00	1.060	2.96E-01	1.05E+00	-1.007	6.61E-01	1.05E+00	1.164	8.29E-02	7.89E-01
<i>Mrc1</i>	Mannose receptor, C type 1	-1.029	2.09E-01	1.09E+00	-1.064	<b>3.72E-02</b>	7.06E-01	1.070	1.50E-01	9.79E-01	1.439	<b>5.63E-05</b>	<b>1.42E-02</b>
<i>Tgfb1</i>	Transforming growth factor, beta 1	1.098	9.24E-02	9.90E-01	-1.085	9.92E-02	9.16E-01	1.196	<b>2.36E-02</b>	5.14E-01	1.093	1.39E-01	9.00E-01
<i>Socs3</i>	Suppressor of cytokine signaling 3	1.037	4.87E-01	1.06E+00	-1.014	5.17E-01	1.06E+00	1.031	5.01E-01	1.08E+00	-1.029	2.80E-01	1.04E+00
<i>Arg1</i>	Arginase 1	-1.017	4.81E-01	1.06E+00	-1.012	5.62E-01	1.06E+00	-1.059	3.59E-01	1.09E+00	-1.091	1.86E-01	9.64E-01
<i>Il10</i>	Interleukin 10	1.026	4.36E-01	1.07E+00	-1.109	1.19E-01	9.53E-01	1.029	5.00E-01	1.08E+00	-1.064	2.52E-01	1.02E+00
<i>Chil3</i>	Chitinase-like 3	1.058	2.19E-01	1.09E+00	-1.100	1.29E-01	9.62E-01	1.066	2.42E-01	1.06E+00	-1.023	3.25E-01	1.06E+00
<i>Il4</i>	Interleukin 4	-1.110	1.71E-01	1.07E+00	1.088	2.62E-01	1.06E+00	-1.004	6.62E-01	1.05E+00	1.099	2.39E-01	9.72E-01
<i>Retnla</i>	Resistin like alpha	-1.003	3.26E-01	1.08E+00	1.010	4.66E-01	1.02E+00	-1.101	1.38E-01	9.77E-01	1.140	1.00E-01	8.33E-01
<i>Cd68</i>	CD68 antigen	1.683	<b>6.74E-08</b>	<b>2.07E-04</b>	-1.201	<b>1.08E-02</b>	4.96E-01	2.042	<b>3.49E-11</b>	<b>1.31E-07</b>	1.292	<b>1.49E-03</b>	1.28E-01
<i>Tyrobp</i>	TYRO protein tyrosine kinase binding protein	1.628	<b>1.75E-07</b>	<b>3.48E-04</b>	-1.237	<b>1.22E-02</b>	5.08E-01	1.570	<b>2.45E-06</b>	<b>1.26E-03</b>	1.129	8.70E-02	7.97E-01
<i>Trem2</i>	Triggering receptor expressed on myeloid cells 2	1.363	<b>8.16E-05</b>	<b>2.93E-02</b>	-1.183	<b>2.46E-02</b>	6.34E-01	1.582	<b>2.06E-06</b>	<b>1.16E-03</b>	1.187	<b>2.56E-02</b>	5.52E-01
<i>Tlr2</i>	Toll-like receptor 2	1.199	<b>1.51E-02</b>	5.48E-01	-1.056	2.77E-01	1.06E+00	1.196	<b>2.15E-02</b>	4.89E-01	1.057	2.35E-01	9.69E-01
<i>P2ry6</i>	Pyrimidinergic receptor P2Y, 6	1.273	<b>2.68E-03</b>	2.45E-01	-1.144	8.74E-02	8.97E-01	1.477	<b>1.64E-05</b>	<b>5.53E-03</b>	1.064	3.39E-01	1.02E+00
<i>Aif1</i>	Allograft inflammatory factor 1 (Iba1)	1.167	<b>2.21E-02</b>	6.37E-01	-1.097	1.53E-01	9.92E-01	1.225	<b>9.88E-03</b>	3.31E-01	1.147	7.10E-02	7.61E-01
<i>Ltb4r1</i>	Leukotriene B4 receptor 1	-1.015	6.22E-01	1.02E+00	-1.007	6.29E-01	1.05E+00	1.011	5.67E-01	1.08E+00	-1.031	5.07E-01	1.10E+00
<i>Tmem119</i>	Transmembrane protein 119	1.060	3.79E-01	1.08E+00	-1.176	5.15E-02	7.79E-01	1.119	1.50E-01	9.79E-01	1.070	3.27E-01	1.01E+00
<i>Siglec1</i>	Sialic acid binding Ig-like lectin 1	1.096	2.04E-01	1.09E+00	-1.102	1.31E-01	9.66E-01	1.145	9.39E-02	8.74E-01	1.061	4.23E-01	1.04E+00